Copy /
RM SL53F26

NACA

RESEARCH MEMORANDUM

for the

U. S. Air Force

LOW-SPEED LONGITUDINAL STABILITY CHARACTERISTICS OF A 1/6-SCALE MODEL OF THE REPUBLIC XF-84H AIRPLANE WITH THE PROPELLER OPERATING

By William C. Sleeman, Jr., and Andrew L. Byrnes, Jr.

Langley Aeronautical Laboratory
Langley Field, Va.

NATIONAL ADVISORY COMMITTEE
FOR AERONAUTICS

WASHINGTON

JUN 24 1953

14

NATIONAL ADVISORY COMMITTEE FOR AERONAUTICS

RESEARCH MEMORANDUM

for the

U. S. Air Force

LOW-SPEED LONGITUDINAL STABILITY CHARACTERISTICS OF A 1/6-SCALE MODEL OF THE REPUBLIC XF-84H AIRPLANE WITH THE PROPELLER OPERATING

By William C. Sleeman, Jr., and Andrew L. Byrnes, Jr.

SUMMARY

A low-speed investigation was made of a 1/6-scale model of the Republic XF-84H airplane. The model had a single tractor propeller and a 40° swept wing of aspect ratio 3.45. This investigation was undertaken to provide information on the effects of propeller operation on longitudinal stability characteristics for the XF-84H airplane and to provide an indication of slipstream effects that might be encountered on similar swept-wing configurations.

Effects of propeller operation were generally destabilizing for all conditions investigated; however, the over-all stability characteristics with power on were greatly dependent on the power-off characteristics. With flaps and slats retracted, longitudinal instability was present at moderate angles of attack both with the propeller off and with power on. The longitudinal stability with flaps and slats deflected, which was satisfactory without power, was decreased by propeller operation, but no marked pitch-up tendency was indicated.

Significant improvement in the power-on stability with flaps retracted was achieved by use of either a wing fence at 75 percent semispan, a leading-edge chord-extension from 65 to 94 percent semispan, or a raised horizontal tail located 65 percent semispan above the thrust line.

INTRODUCTION

At the request of the U. S. Air Force, a series of tests was made in the Langley 300 MPH 7- by 10-foot tunnel of a 1/6-scale model of the Republic XF-84H airplane which is a fighter-type airplane driven by a single supersonic propeller. The configuration tested had a 40° swept-back wing of aspect ratio 3.45. Propeller-off results for the model are presented in reference 1. This paper presents the effects of propeller operation and wing and tail modifications on static longitudinal stability characteristics of the model with power on.

Although procedures for estimating the effects of propeller operation have been developed for unswept configurations, there is little information on the applicability of such procedures to configurations having appreciable wing sweep. The present investigation accordingly was undertaken to provide information on the effects of power on longitudinal stability of the original Republic XF-84H configuration and also to afford general information on slipstream effects that might be encountered on similar swept-wing configurations. Additional power-on information was obtained by using some of the most beneficial modifications (wing fence, leading-edge chord-extension, and raised horizontal tail) found in the extensive power-off investigation reported in reference 1.

Only a brief analysis of the results of this investigation has been made in order to expedite the publishing of the data.

COEFFICIENTS AND SYMBOLS

The data obtained in this investigation are presented as standard NACA coefficients of forces and moments about the stability axes. The system of axes employed, together with an indication of positive forces, moments, and angular displacements, is presented in figure 1. Moment coefficients are given about the center-of-gravity location shown in figure 2 (15 percent mean aerodynamic chord, on the thrust line).

The coefficients and symbols are defined as follows:

C_L lift coefficient, Lift/qS

C_X longitudinal-force coefficient, X/qS

C_m pitching-moment coefficient, $M/qS\bar{c}$

X longitudinal force along X-axis (Drag = -X), lb

Z	force along Z-axis (Lift = -Z), lb
M	pitching moment about Y-axis, ft-lb
T_c	effective-thrust disk-loading coefficient, $T_e/\rho V^2 D^2$
Q_c	torque disk-loading coefficient, $Q/\rho V^2 D^3$
V/nD	propeller advance-diameter ratio
η	propulsive efficiency, $T_e V/2\pi nQ$
T_e	effective propeller thrust, lb
Q	propeller torque, ft-lb
q	free-stream dynamic pressure, $\frac{1}{2}\rho V^2$, lb/sq ft
V	free-stream velocity, ft/sec
ρ	air density, slugs/cu ft
S	wing area, sq ft (9.03 on model, excluding area of inlet ducts)
$\bar{c}$	wing mean aerodynamic chord, ft (1.67 on model)
c	local streamwise chord, ft
b	wing span, ft; also, in figure 7, propeller blade section chord, ft
D	propeller diameter, ft (2.00 on model)
R	propeller radius, ft
r	radius to any propeller blade element, ft
h	propeller blade section maximum thickness, ft
n	propeller rotational speed, rps
α	aerodynamic angle of attack of thrust line, deg
α_g	geometric angle of attack of thrust line, deg
β	propeller blade angle, deg

i_t stabilizer incidence relative to thrust line, positive when trailing edge is down, deg

ϵ effective downwash angle at horizontal tail and local upwash angle in propeller plane, deg

δ_f flap deflection, deg

σ tail effectiveness parameter, $\left(\frac{\partial C_m}{\partial i_t}\right)_{\text{wing on}} \Big/ \left(\frac{\partial C_m}{\partial i_t}\right)_{\text{max,wing off}}$

MODEL AND APPARATUS

The basic model used in this investigation was a 1/6-scale model of the Republic XF-84H airplane. The wing had 40° sweepback of the quarter-chord line, aspect ratio 3.45, taper ratio 0.578, and had NACA 64A010 airfoil sections normal to the quarter-chord line. A two-view drawing of the model is presented in figure 2 and a photograph of the model installed in the Langley 300 MPH 7- by 10-foot tunnel is given as figure 3. Tabulated geometric characteristics of the basic configuration are given in table I. The model was supplied by Republic Aviation Corporation and was not checked for accuracy.

Differences in the model and proposed airplane configuration are indicated in figure 2 by dashed lines. Since no attempt was made to simulate air flow through the model, the inlets and jet exit were faired over as shown. It was not feasible to duplicate the nonrotating propeller spinner nose on the model and a hemispherical spinner nose was used instead. The thrust line of the model coincided with the fuselage center line, whereas the airplane design is to incorporate 1° of downward tilt of the thrust axis relative to the fuselage center line.

Effects of several modifications were studied to alleviate the pitch-up tendency found in the basic flap-retracted configuration. Details of the wing fence and leading-edge chord-extension tested are shown in figures 4 and 5 and a drawing of the high tail position is given as figure 6.

Geometric characteristics of the solid-steel model propeller are given in figure 7. The blade angle used in all tests was 16.5° at 0.75R and was selected on the basis of simulating the thrust-torque relationship for the airplane at maximum power and high thrust. The propeller was driven by a 47-horsepower electric motor in the model. The rotational speed of the propeller was determined by observation of a

stroboscopic-type frequency indicator which indicated the output frequency of a small alternator connected to the motor shaft. The accuracy of the frequency indicator was within ±0.05 percent.

Some flow studies were made in the region of the tail by means of a tuft grid located approximately 1.5 wing semispans behind the reference center of gravity. A description of the tuft grid is given in reference 2. The horizontal and vertical tails were replaced by unswept 1/8-inch-diameter rods which indicated the location of the vertical tail, the two horizontal-tail positions used in this investigation, and a low tail position 7 percent b/2 below the thrust line.

Upwash surveys in the propeller plane were made with an angularity survey rake mounted on the left side of the fuselage and a static-pressure rake on the right side. A drawing of the apparatus used in the upwash surveys is presented in figure 8.

TESTS AND RESULTS

Test conditions.- Tests were made in the Langley 300 MPH 7- by 10-foot tunnel at dynamic pressures of 8 pounds per square foot for power-on tests and 40 pounds per square foot for propeller-off tests. These conditions correspond to airspeeds of approximately 56 and 126 miles per hour and to test Reynolds numbers of approximately 0.9×10^6 and 2.0×10^6, respectively, based on the wing mean aerodynamic chord of 1.67 feet.

The wing-off tests, propeller calibrations, and upwash surveys were made with the model mounted on a single centrally located vertical support strut. All other tests were made with the model supported by its wings through a twin-strut system as indicated in figure 3. The presence of the wing support struts prevented the use of the main landing wheels and therefore tests of the flap-deflected configuration (landing condition) were made with only the nose wheel extended.

Test procedure.- A propeller calibration was made with the propeller on the clean fuselage (wing, canopy, dorsal, empennage, and tail skid removed) and these results are presented in figure 9. The propeller was calibrated by measuring the resultant longitudinal force, minimum motor current, and rolling moment of the model at 0° angle of attack for a range of propeller speeds. Effective propeller thrust was computed from the following relationship

$$T_e = X_R - X_o$$

where X_R is the longitudinal force obtained with the propeller operating and X_o is the longitudinal force of the model with the propeller removed.

Torque coefficients presented in figure 9 were obtained from measured rolling moments and these results were in excellent agreement with those determined by use of a calibration of motor torque as a function of minimum current.

Some of the power-on tests simulated constant-power flight conditions in which the propeller speed and angle of attack of the model were adjusted to correspond to the relationship of T_c and C_L given in figure 10. The power conditions of figure 10 are for a gross weight of 16,000 pounds at sea-level altitude and were selected to simulate the most extreme constant-power flight conditions that might be encountered on this airplane. Power A represents the military power rating of 7,070 horsepower and power B (approach power) is 60 percent of normal power.

For the constant-thrust tests, the propeller speed was held constant while the angle of attack of the model was varied. The propeller and spinner were replaced by a dummy spinner for the propeller-off tests.

The vertical tail was on the model during all tests except those of the fuselage alone.

Corrections.- Jet-boundary corrections to the angles of attack, longitudinal-force coefficients, and tail-on pitching-moment coefficients were obtained from reference 3. Jet-boundary corrections to the upwash angles were obtained from reference 2 for wing-on surveys. The following corrections were added to the data

$$\Delta\alpha = 1.02C_{L_W} \text{ (degrees)}$$

$$\Delta C_x = -0.0155C_{L_W}{}^2$$

$$\Delta C_m = -7.39C_{L_W}\left(\frac{0.220}{\sqrt{\sigma}} - 0.116\right)\frac{\partial C_m}{\partial i_t}$$

$$\Delta\epsilon = -0.25C_{L_W} \text{ (degrees upwash)}$$

where

$$C_{L_W} = C_L - (\Delta C_L)_{\text{propeller thrust}}$$

and

$$(\Delta C_L)_{\text{propeller thrust}} = T_c \frac{2D^2}{S} \sin \alpha_g$$

No systematic evaluation of support tares has been made and corrections for support interference were not applied to the data. Results of a few tare tests, however, have indicated that the wing support tares were small and associated primarily with a small change in longitudinal trim. Single support tares were evaluated for the propeller calibrations and were found to be negligible for resultant longitudinal-force coefficients. Blockage corrections have not been applied to the data.

Results.- The figures presenting the longitudinal-stability results are as follows:

DISCUSSION

Basic Configuration

Fuselage alone.- Pitching-moment results of figure 11 were obtained to determine the magnitude of the destabilizing normal-force effect of the windmilling propeller. The thrust coefficient of the windmilling propeller was $T_c = -0.027$. The experimental change in $\partial C_m/\partial \alpha$ due to the windmilling propeller was 0.0023 which compares favorably with a value of 0.0020 estimated from reference 4. These results were obtained with the wing, canopy, and other external protuberances removed from the fuselage. Other wing-off results with and without the horizontal tail were presented in reference 1 on the same basic configuration; however, these data were obtained with the vertical tail, canopy, and so forth on the fuselage.

Basic model.- The propeller-off results of figure 12 indicate undesirable longitudinal-stability characteristics with flaps retracted for lift coefficients from $C_L = 0.7$ to 0.9. The causes for this behavior and means for alleviating the pitch-up tendency were treated extensively in reference 1. Application of constant-thrust power caused an initial stability loss at low lift, and the high-lift instability encountered without power persisted with power on (figs. 13(a), 13(b), and 20(a)). Characteristics of the model with power A were even more undesirable than with constant T_c at higher lift coefficients due to the increasing thrust coefficient with lift coefficient (figs. 13(c) and 20(a)). These adverse characteristics were primarily associated with the effects of an extremely large increase in downwash gradient, which for power-on conditions was further increased by the higher lift effectiveness of the tail immersed in the slipstream. (See fig. 14 and tuft grid photographs, fig. 21.)

For the flap-deflected and slats-extended condition, acceptable stability characteristics are indicated through the lift range without power (fig. 15). Application of constant power caused a considerable reduction in stability at high lift (fig. 16); however, no marked pitch-up tendency was indicated up to the highest lift attained. For the power B condition, pitching-moment results without the horizontal tail (fig. 16) were not presented because the wind-off values were believed to be in error.

Modifications to the Basic Configuration, $\delta_f = 0^\circ$

The longitudinal-stability difficulties encountered with power on appeared to be associated with inherent deficiencies in the power-off stability characteristics, rather than being attributed to large direct

adverse propeller effects. It was therefore believed that significant improvement in the power-on characteristics could be effected by utilizing some of the beneficial modifications developed for the power-off configuration (ref. 1). Effects of the various modifications tested (figs. 17, 18, and 19) are summarized in figure 20(b) for $T_c = 0.66$ and the over-all results are representative of those obtained with both power conditions tested.

The addition of a wing fence at 75 percent wing semispan or the leading-edge chord-extension from 65 to 94 percent semispan showed little effect (fig. 20(b)) on the constant-thrust stability up to the lift coefficient where pitch-up was indicated for the basic model ($C_L = 0.9$). Significant benefits of both modifications were shown for the higher lift range; however, an abrupt pitch-up tendency was indicated near the maximum lift attained for both modifications. It appears that the chord-extension was somewhat more effective than the fence in delaying the onset of high-lift instability. This relative behavior was also indicated in the results of reference 1.

The stabilizing effect of raising the horizontal tail (figs. 19 and 20(b)) is most pronounced at low and moderate lift coefficients due to relatively small downwash changes with angle of attack. (See tuft grid photographs, fig. 21.) The significant stability gains attributed to the high tail diminished at high angles of attack; however, the onset of power-on instability was delayed to a higher lift coefficient than for the basic model (fig. 20(b)). These characteristics were also evident with the high tail with the propeller removed (ref. 1). This high-lift instability appears to be associated with the unfavorable downwash variation encountered as the tail approaches the level of the rolled-up wing vortices (fig. 21).

Flow Surveys in the Propeller Plane

Results of upwash surveys made along a horizontal line through the thrust axis in the propeller plane are presented in figure 22 for the wing and fuselage and the fuselage alone. Data are not presented for survey positions outboard of the 0.75R station because of difficulties with the survey rake. Upwash gradients estimated by the method of reference 5 are compared with experimental results in figure 23. The effect of sweep was included in the estimate of wing upwash contribution. In general, estimated and experimental data compare favorably; however, the effect of the wing is somewhat higher than would be estimated.

CONCLUSIONS

An investigation of the low-speed longitudinal stability characteristics of a 1/6-scale model of the Republic XF-84H airplane with the propeller operating indicated the following conclusions:

1. The effects of propeller operation were generally destabilizing for all conditions investigated; however, the over-all stability characteristics with power on were greatly dependent on the power-off characteristics.

2. With flaps retracted, the longitudinal instability at moderate angles of attack for the basic power-off condition persisted when power was applied.

3. Longitudinal stability with flaps and slats deflected, which was satisfactory without power, was decreased by propeller operation but no marked pitch-up tendency was indicated.

4. A wing fence at 75 percent semispan or a leading-edge chord-extension from 65 to 94 percent semispan improved the power-on stability characteristics of the basic model. The chord-extension was found to be the most beneficial in that the point of high-lift instability was delayed to a higher lift than could be obtained by any other modification tested.

5. Raising the horizontal tail to 65 percent wing semispan above the thrust axis increased the initial low-lift stability and delayed the onset of power-on instability.

Langley Aeronautical Laboratory,
National Advisory Committee for Aeronautics,
Langley Field, Va., June 12, 1953.

Joseph Weil
for William C. Sleeman, Jr.
Aeronautical Research Scientist

Andrew L. Byrnes, Jr.
Aeronautical Research Scientist

Approved: Thomas A. Harris
Thomas A. Harris
Chief of Stability Research Division

mjw

REFERENCES

1. Weil, Joseph, Sleeman, William C., Jr., and Byrnes, Andrew L., Jr.: Investigation of the Effects of Wing and Tail Modifications on the Low-Speed Stability Characteristics of a Model Having a Thin 40° Swept Wing of Aspect Ratio 3.5. NACA RM L53C09, 1953.

2. Sleeman, William C., Jr., and Linsley, Edward L.: Low-Speed Wind-Tunnel Investigation of the Effects of Propeller Operation at High Thrust on the Longitudinal Stability and Trim of a Twin-Engine Airplane Configuration. NACA RM L52D04, 1952.

3. Gillis, Clarence L., Polhamus, Edward C., and Gray, Joseph L., Jr.: Charts for Determining Jet-Boundary Corrections for Complete Models in 7- by 10-Foot Closed Rectangular Wind Tunnels. NACA WR L-123, 1945. (Formerly NACA ARR L5G31.)

4. Ribner, Herbert S.: Notes on the Propeller and Slipstream in Relation to Stability. NACA WR L-25, 1944. (Formerly NACA ARR L4I12a.)

5. Yaggy, Paul F.: A Method for Predicting the Upwash Angles Induced at the Propeller Plane of a Combination of Bodies With an Unswept Wing. NACA TN 2528, 1951.

TABLE I

Summary of Basic Model Geometry

Wing:	
Area (not including inlet area), sq ft	9.03
Span, ft	5.59
Sweepback of quarter-chord line, deg	40
Aspect ratio	3.45
Taper ratio	0.578
Dihedral	-3°30'
Incidence	2°30'
Geometric twist, deg	0
Mean aerodynamic chord, ft	1.67
Airfoil section (normal to quarter-chord line)	NACA 64A010
Root chord, ft	2.063
Tip chord, ft	1.195
Flap:	
Type	Plain trailing edge
Area (one flap), sq ft	0.420
Span, ft	1.009
Hinge line, percent c	75
Maximum deflection, deg	40
Aileron:	
Area (one aileron), sq ft	0.38
Span, ft	1.24
Hinge line, percent c	75
Maximum deflection (normal to hinge line), deg	±18
Leading-edge slat:	
Span of one slat (normal to model center line), ft	1.33
Ratio of slat chord to wing chord (normal to c/4)	0.140
Inboard edge (from model center line), ft	1.347
Forward extension of slat, percent c	8.4
Downward extension of slat, percent c	7.24

TABLE I - Concluded

Summary of Basic Model Geometry

Horizontal tail:	
Type	All-movable
Area, sq ft	1.55
Span, ft	2.36
Sweepback (quarter-chord line), deg	40
Aspect ratio	3.59
Taper ratio	1.0
Dihedral, deg	0
Chord, ft	0.67
Deflection range, deg	-6 to 15
Airfoil section (normal to leading edge)	NACA 64A009
Tail length (c.g. to quarter mean aerodynamic chord of horizontal tail), ft	3.808
Vertical tail:	
Area, sq ft	1.73
Span, ft	1.815
Sweepback of quarter-chord line	41°16'10"
Aspect ratio	1.90
Taper ratio	0.340
Mean aerodynamic chord	0.955
Airfoil section (normal to quarter-chord line)	NACA $64_{(10)}$A011

NACA-Langley - 6-23-53 - 50

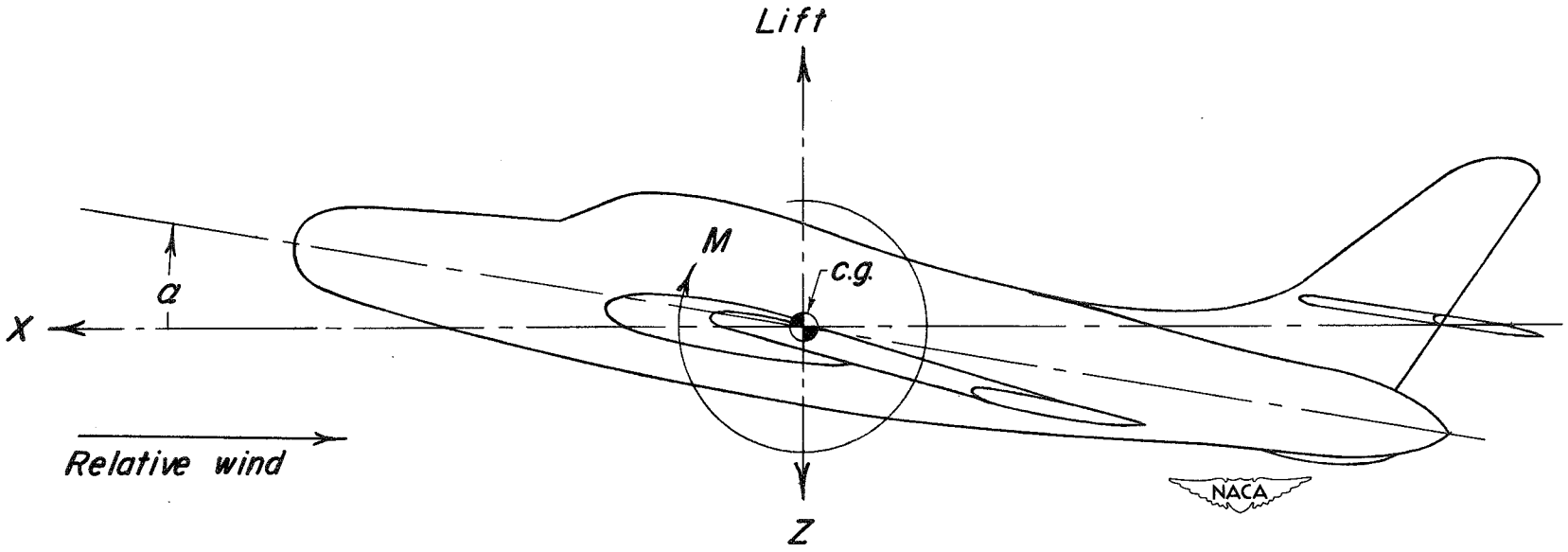

Figure 1.- System of axes; positive values of forces, moments, and angles are indicated by arrows.

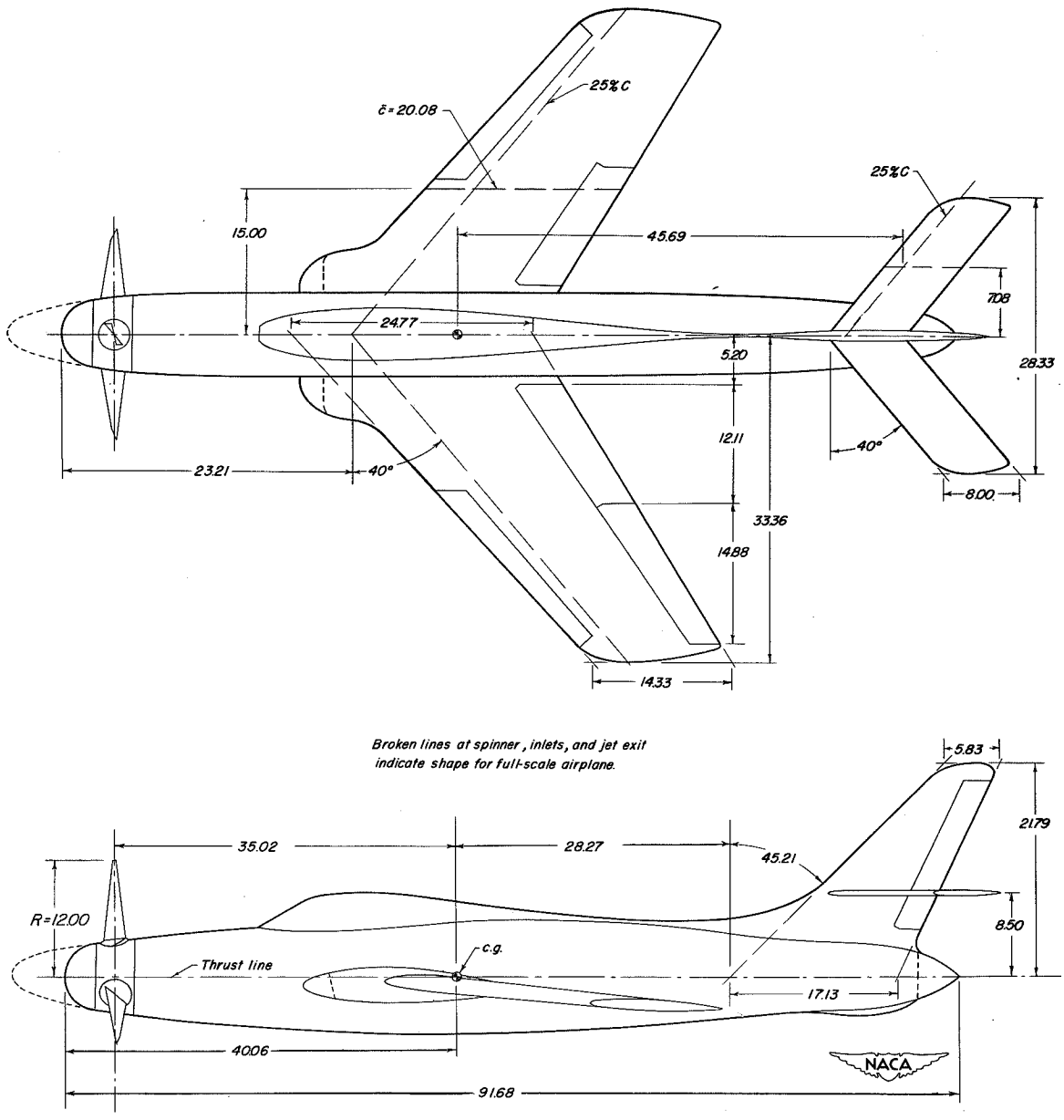

Figure 2.- Two-view drawing of a 1/6-scale model of the original Republic XF-84H airplane configuration. All dimensions are in inches.

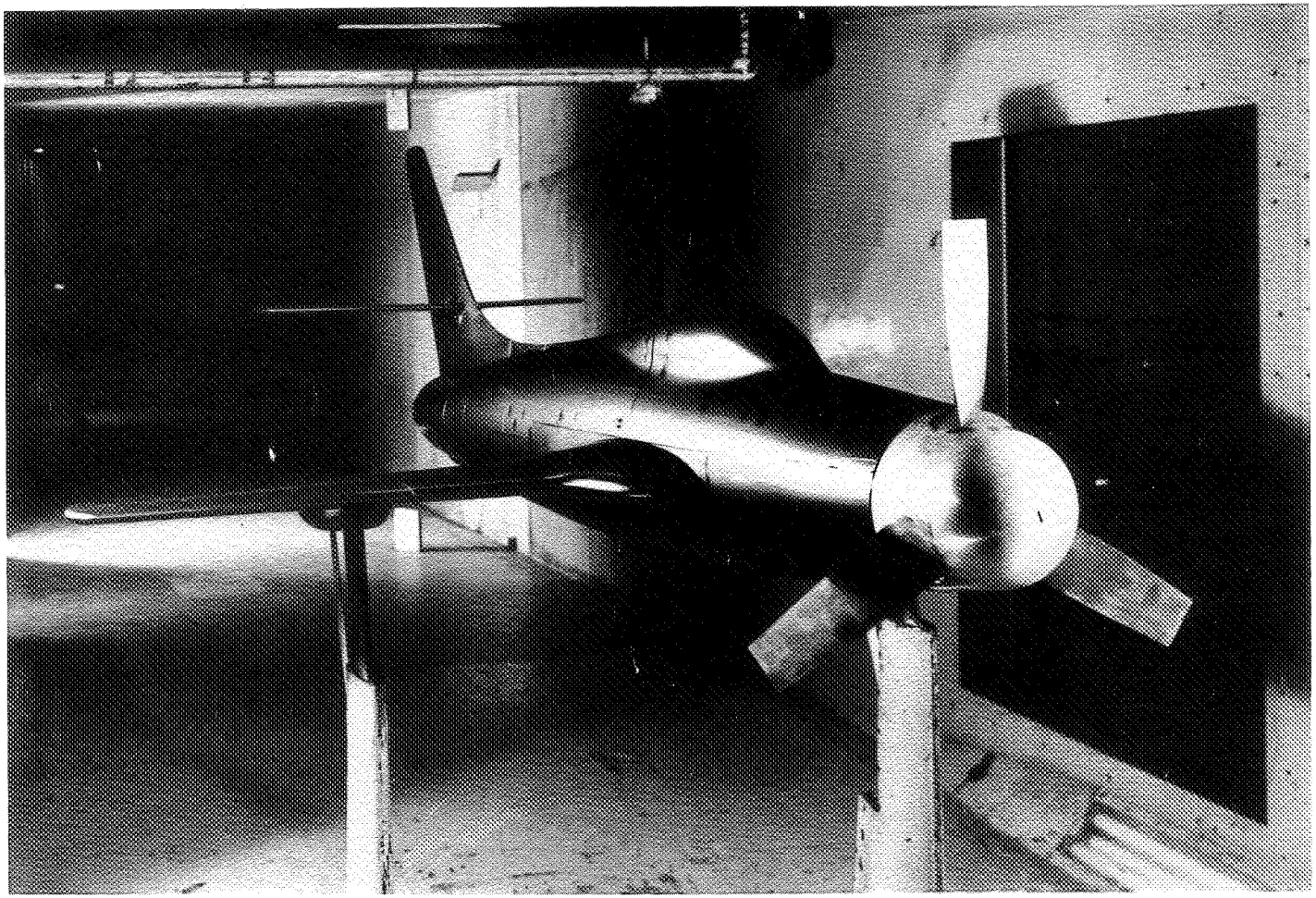

L-75003

Figure 3.- Photograph of the 1/6-scale model of the original Republic XF-84H airplane configuration mounted in the Langley 300 MPH 7- by 10-foot tunnel.

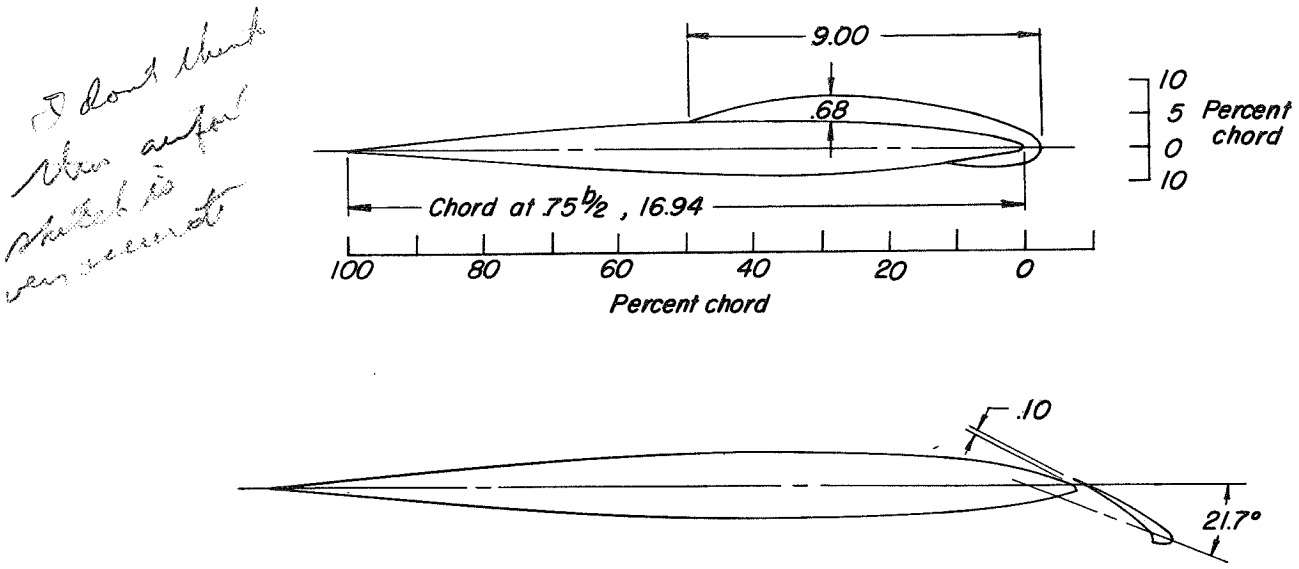

A-A Typical streamwise section showing extended slat position

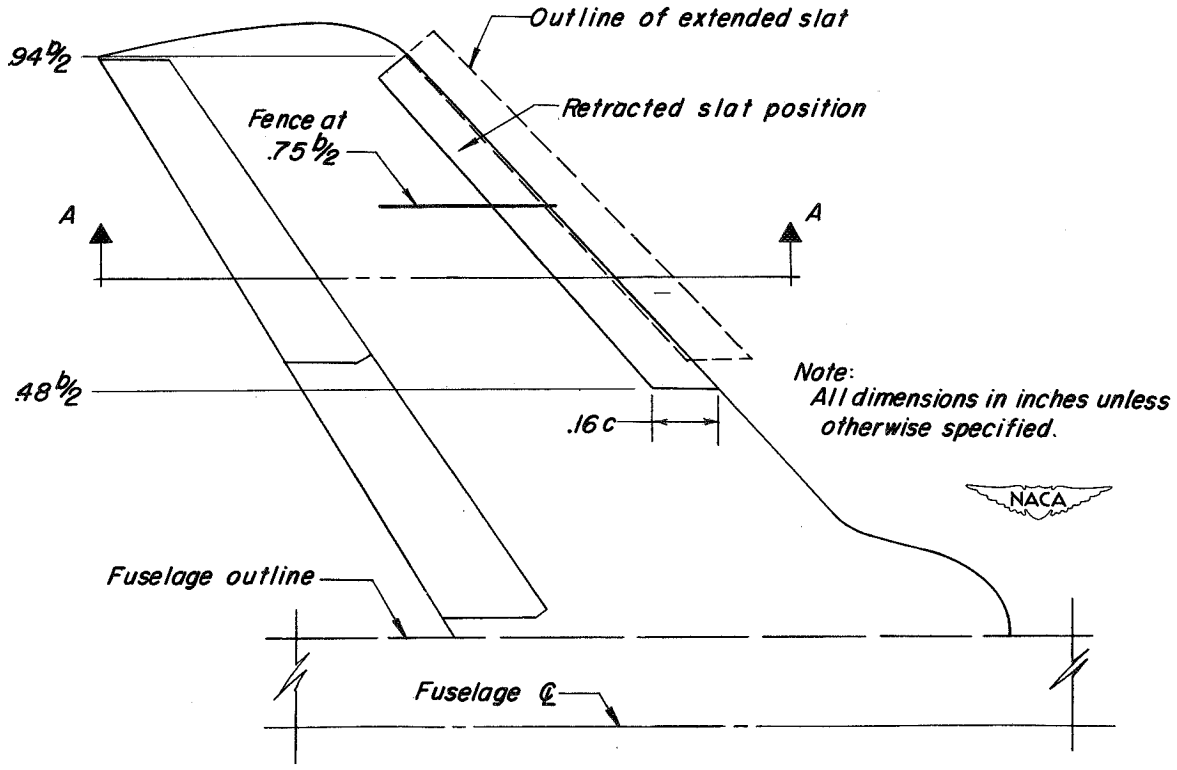

Figure 4.- Details of the slat and wing fence investigated.

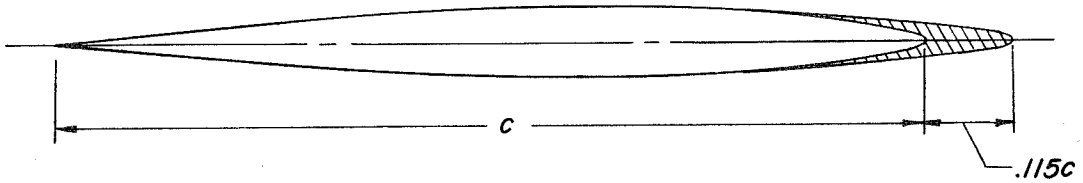

A-A Typical streamwise section showing leading-edge extension

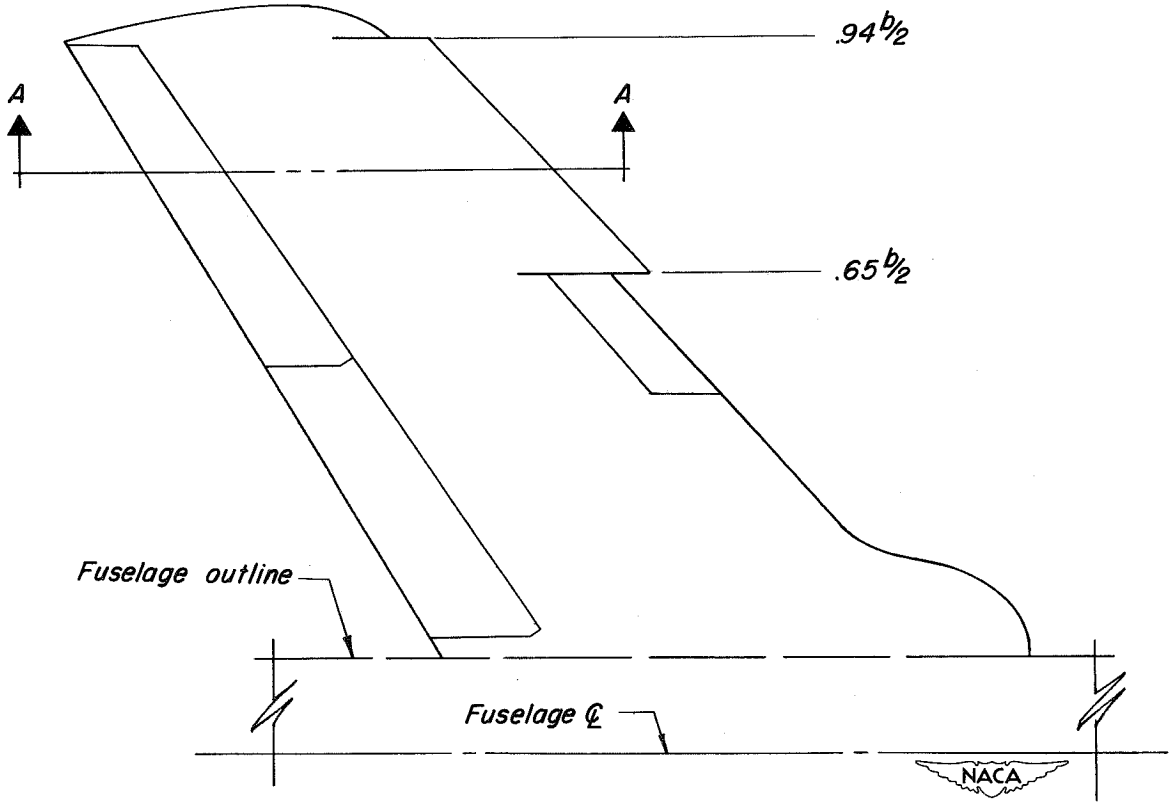

Figure 5.- Details of the leading-edge chord-extension investigated.

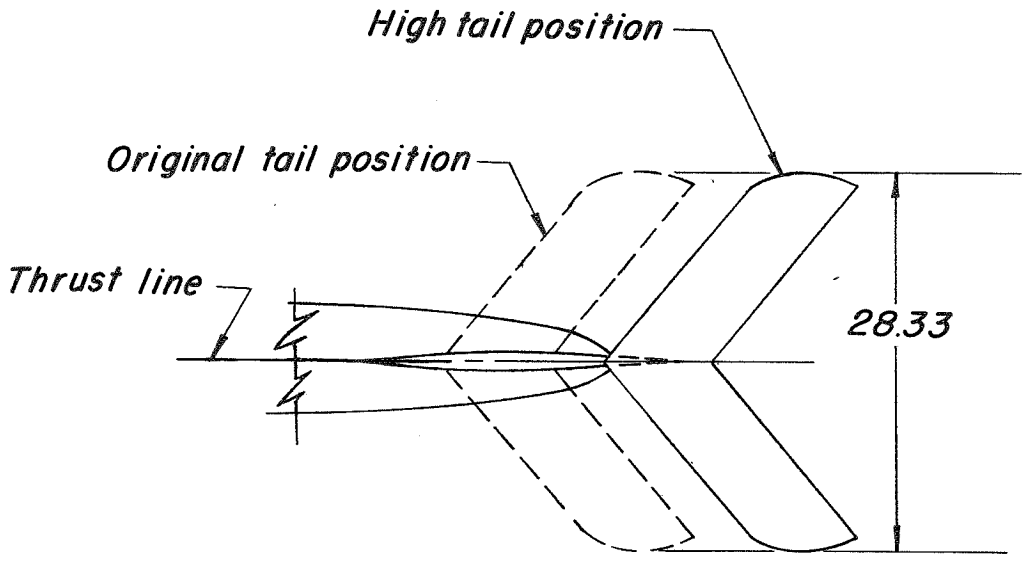

Dimensions in inches.

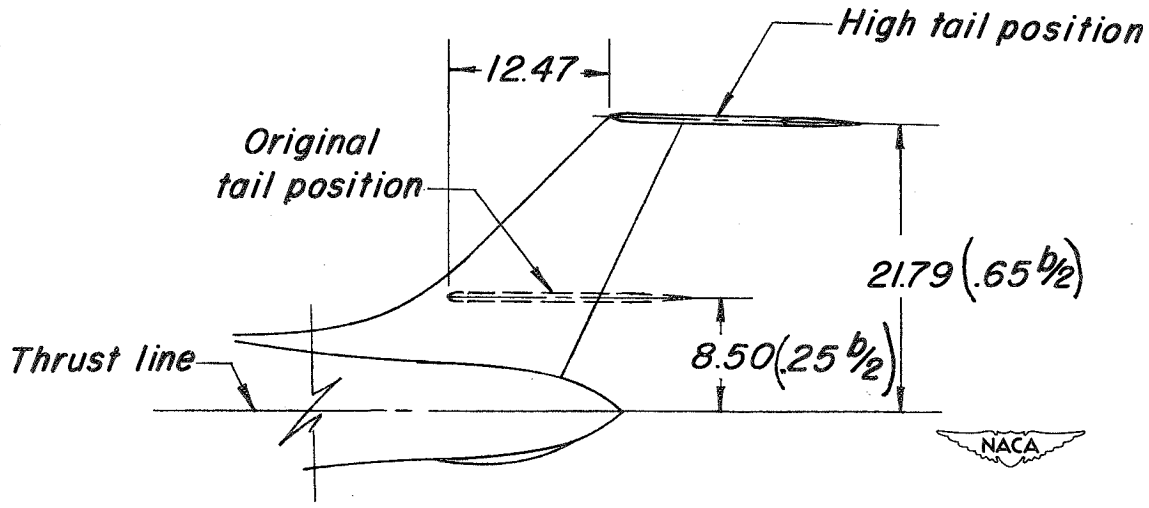

Figure 6.- Horizontal-tail configurations investigated.

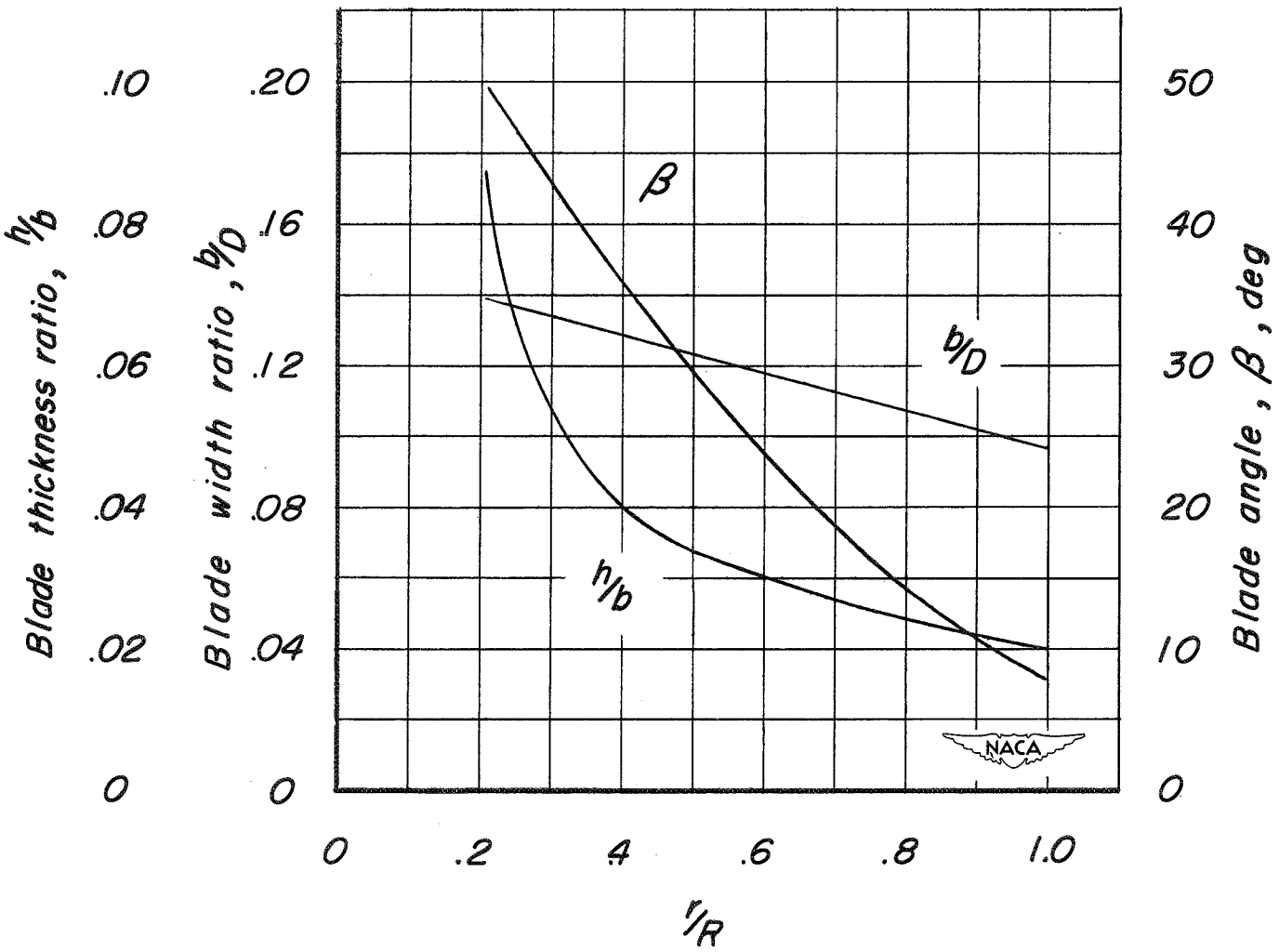

Figure 7.- Blade-form characteristics of the model propeller.

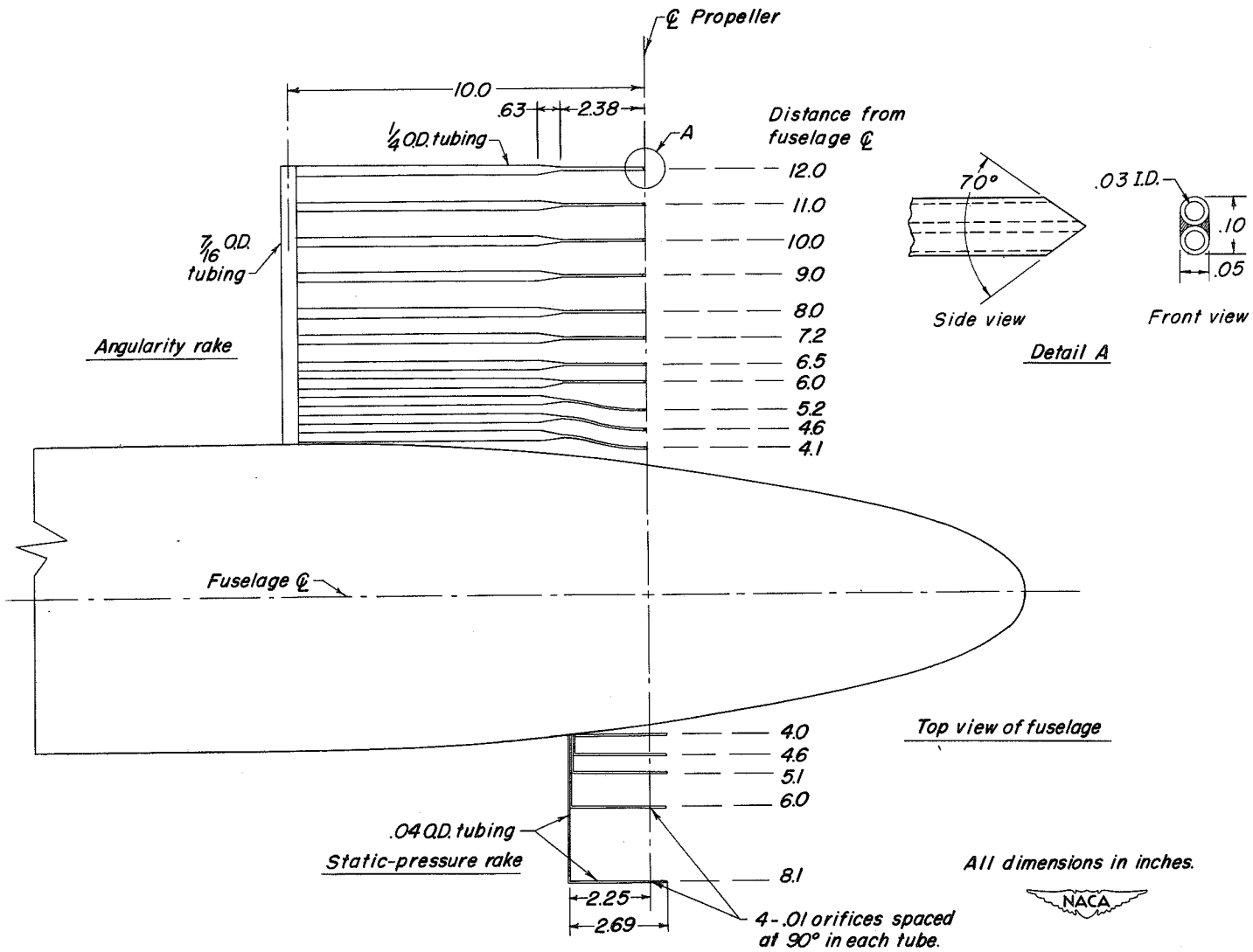

Figure 8.- Details of rake used in upwash surveys.

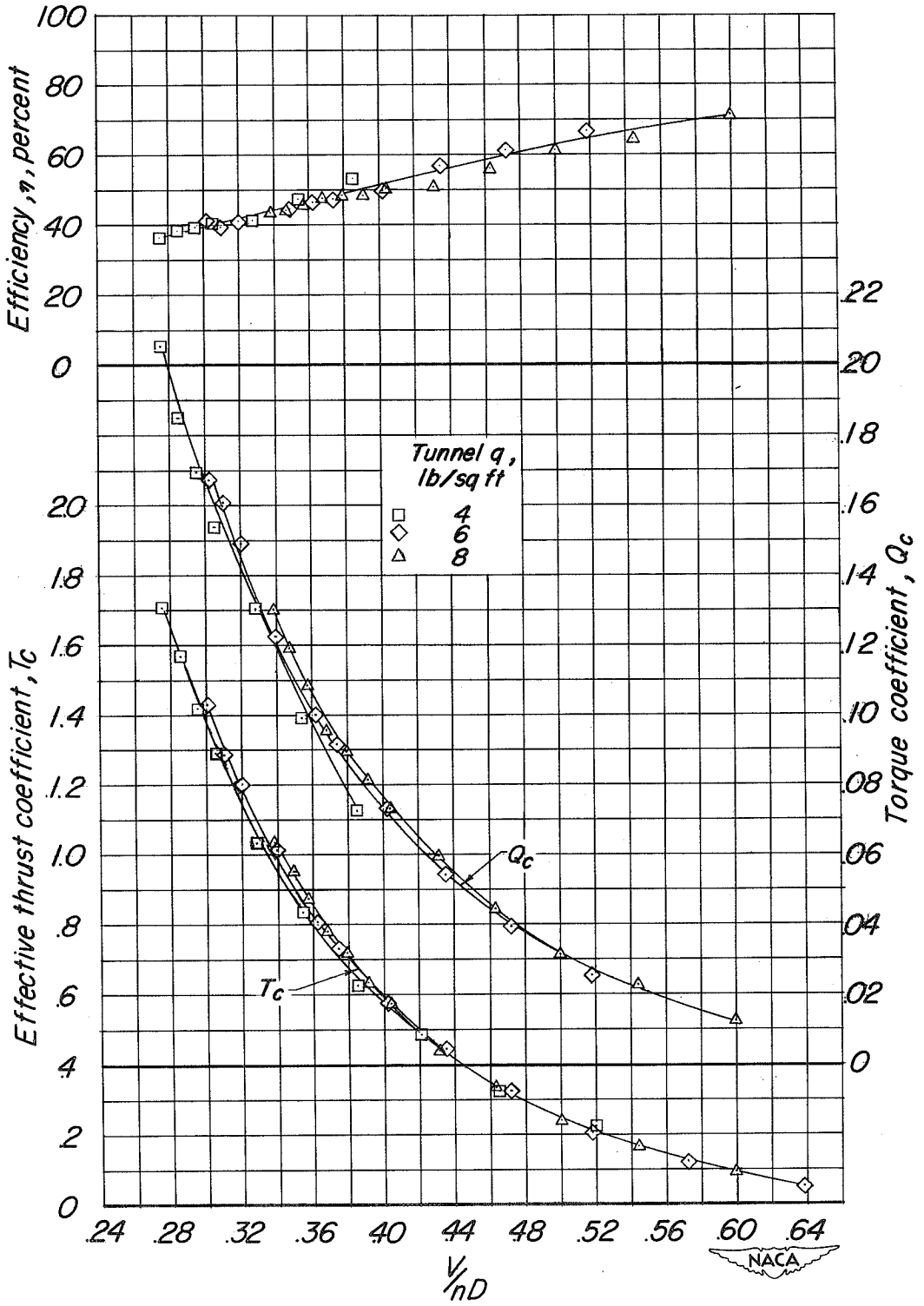

Figure 9.- Characteristics of the model propeller as determined from calibrations with the propeller on the basic fuselage. Wing, tail, canopy, and external protuberances removed. $\beta_{0.75R} = 16.5°$.

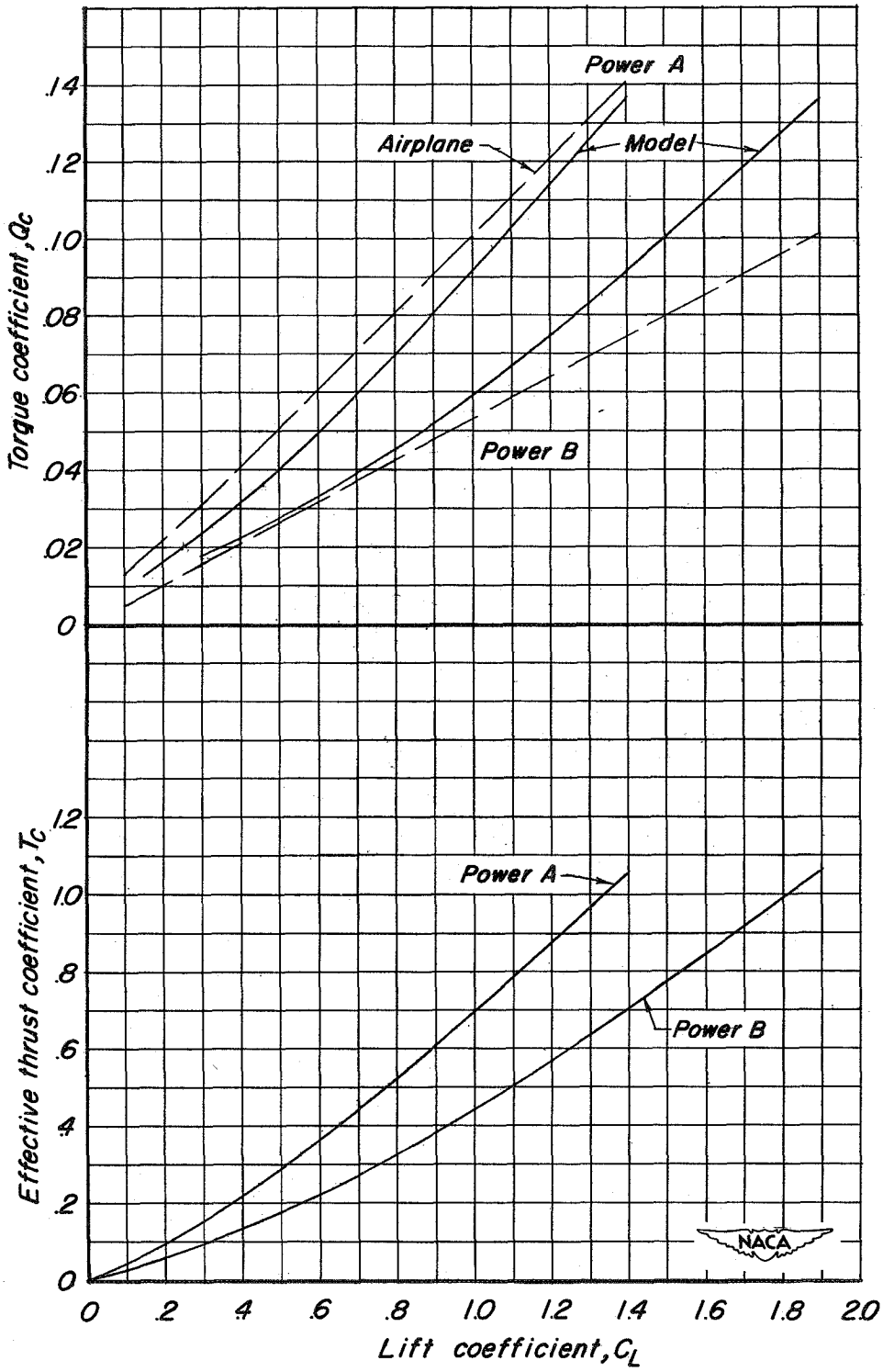

Figure 10.- Variation of effective thrust coefficient and torque coefficient with lift coefficient for the constant power conditions investigated.

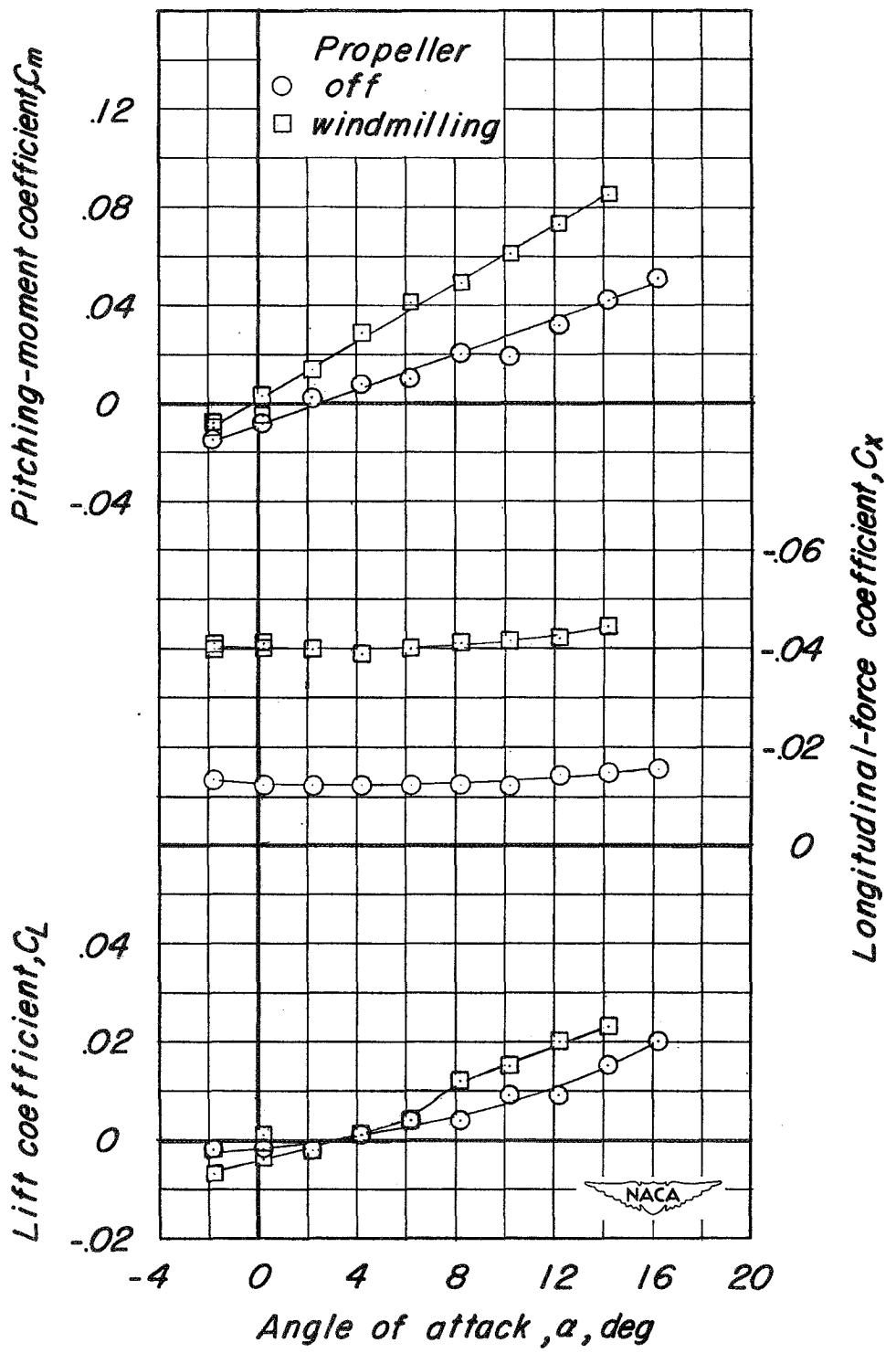

Figure 11.- Effect of the windmilling propeller on the aerodynamic characteristics in pitch of the basic fuselage. Test dynamic pressure q = 20 pounds per square foot. Canopy and external protuberances removed.

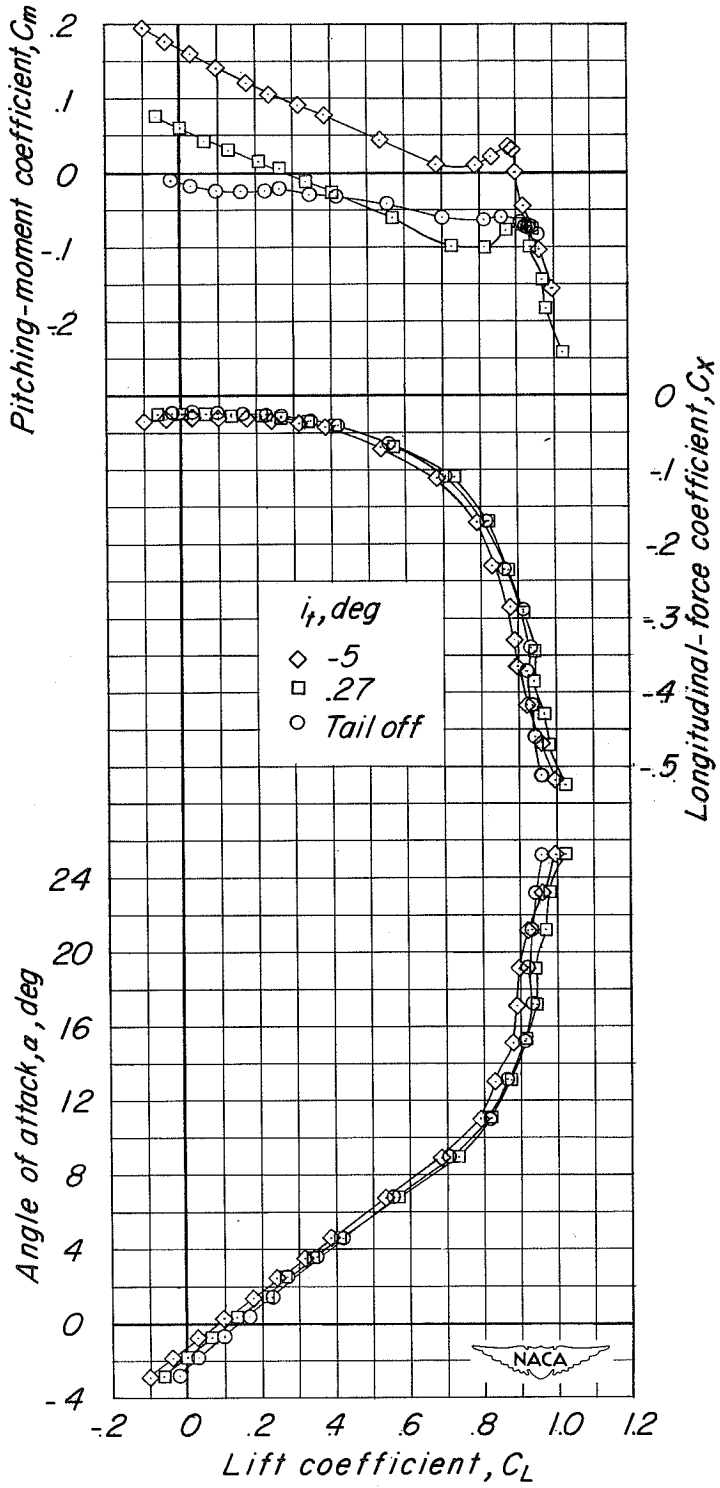

Figure 12.- Effect of stabilizer incidence on the aerodynamic characteristics of the complete model. Propeller off; $\delta_f = 0^\circ$; original configuration.

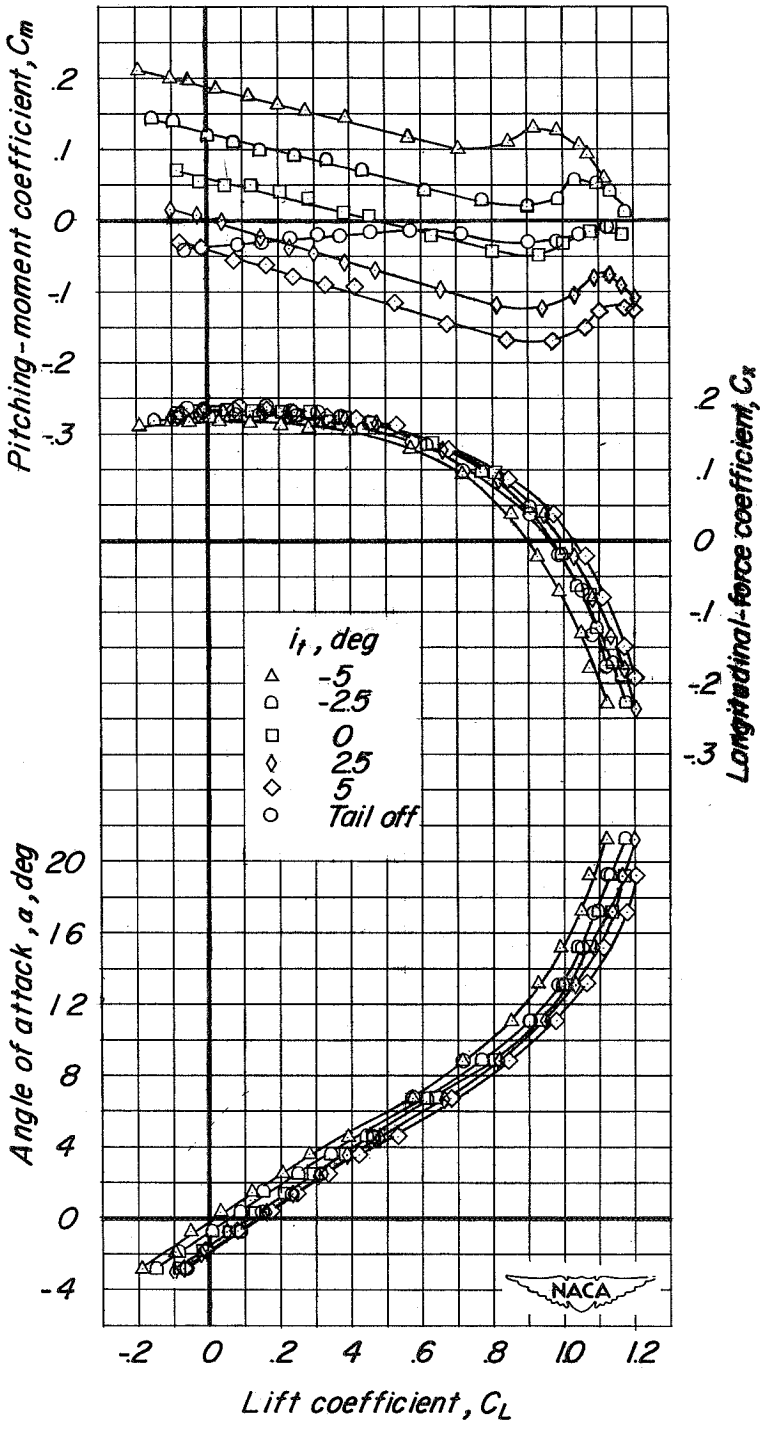

(a) $T_c = 0.22$.

Figure 13.- Effect of stabilizer incidence on the aerodynamic characteristics of the complete model with the propeller operating. Original configuration; $\delta_f = 0^\circ$.

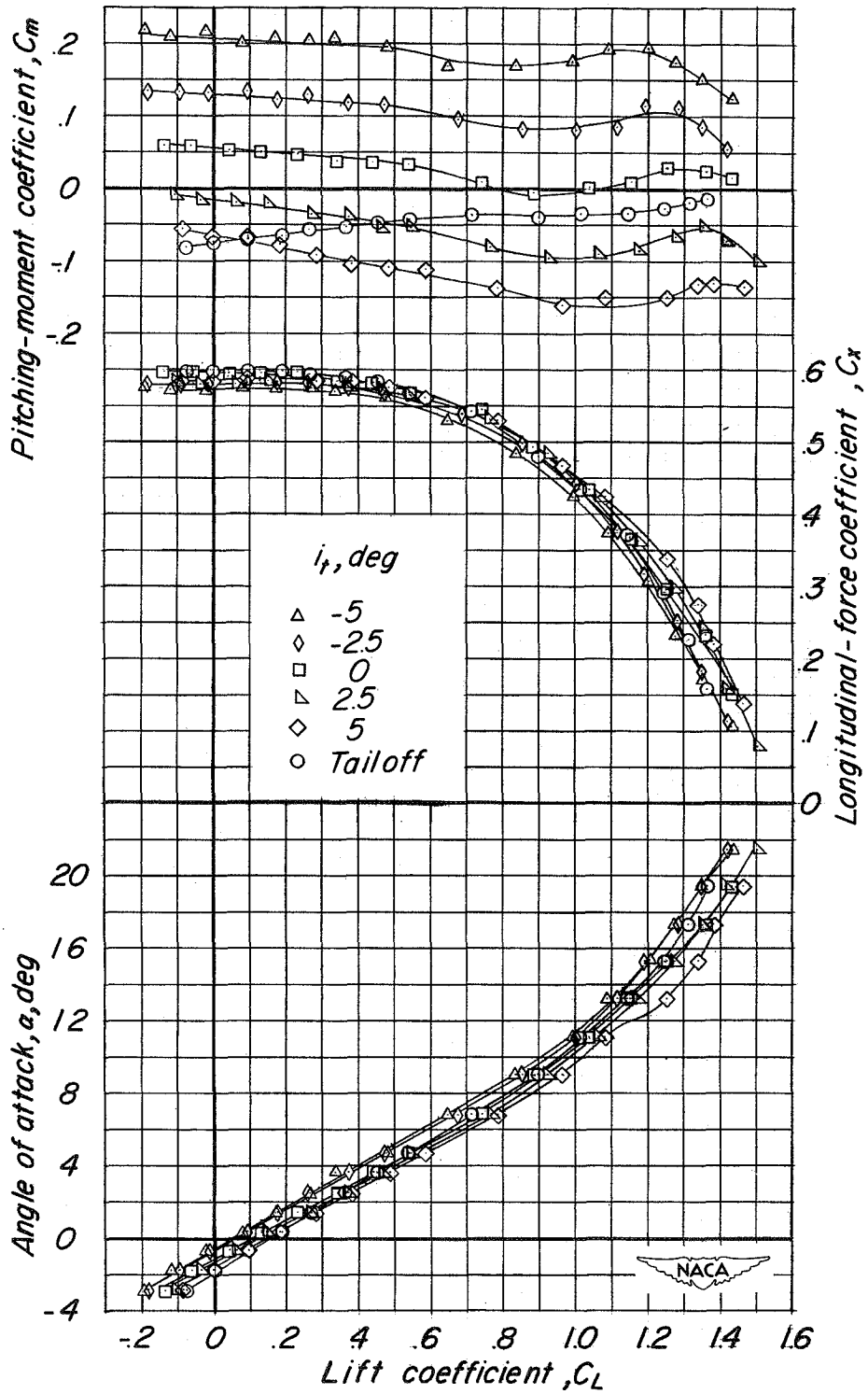

(b) $T_c = 0.66$.

Figure 13.- Continued.

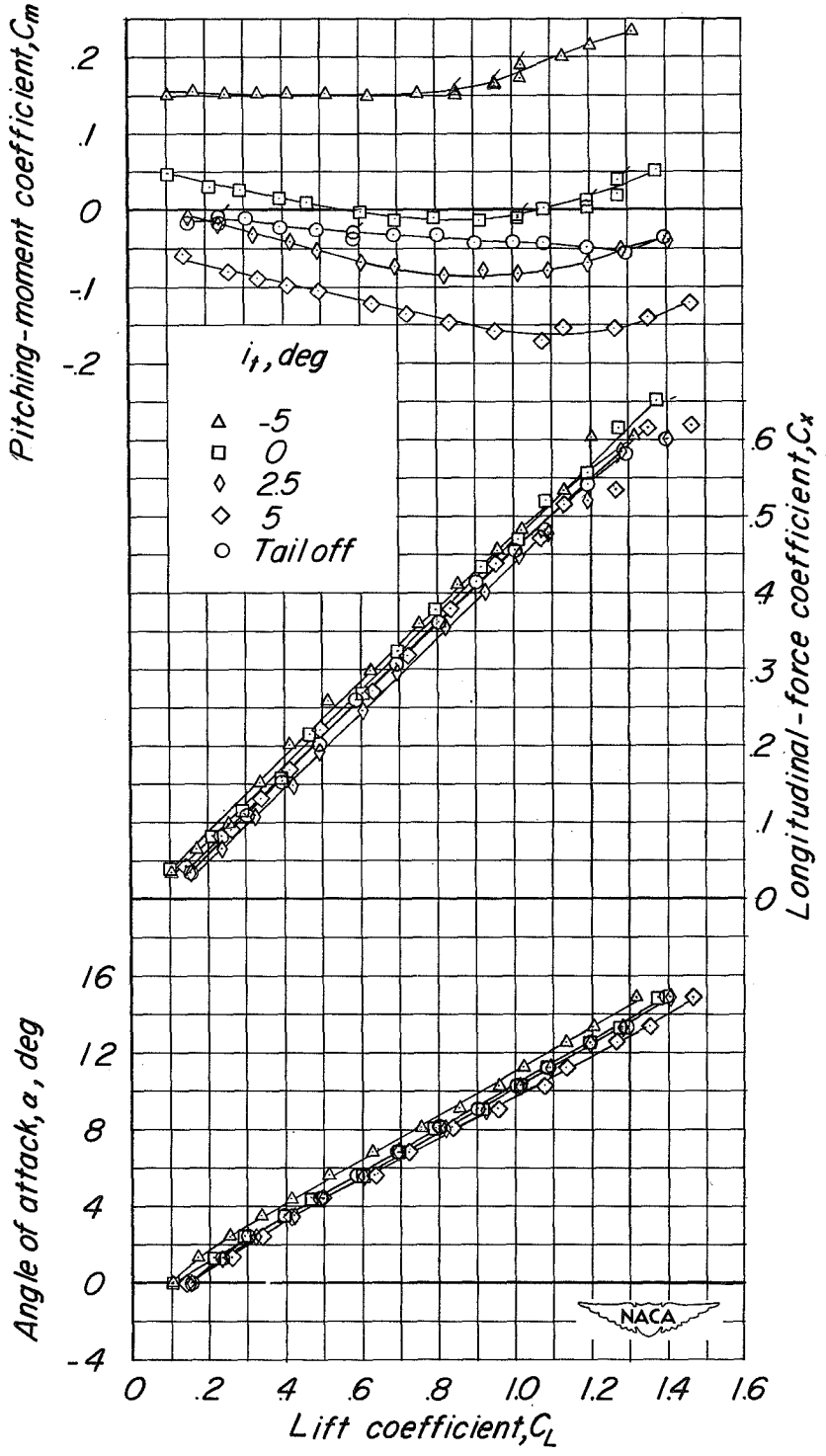

(c) Power A.

Figure 13.- Concluded.

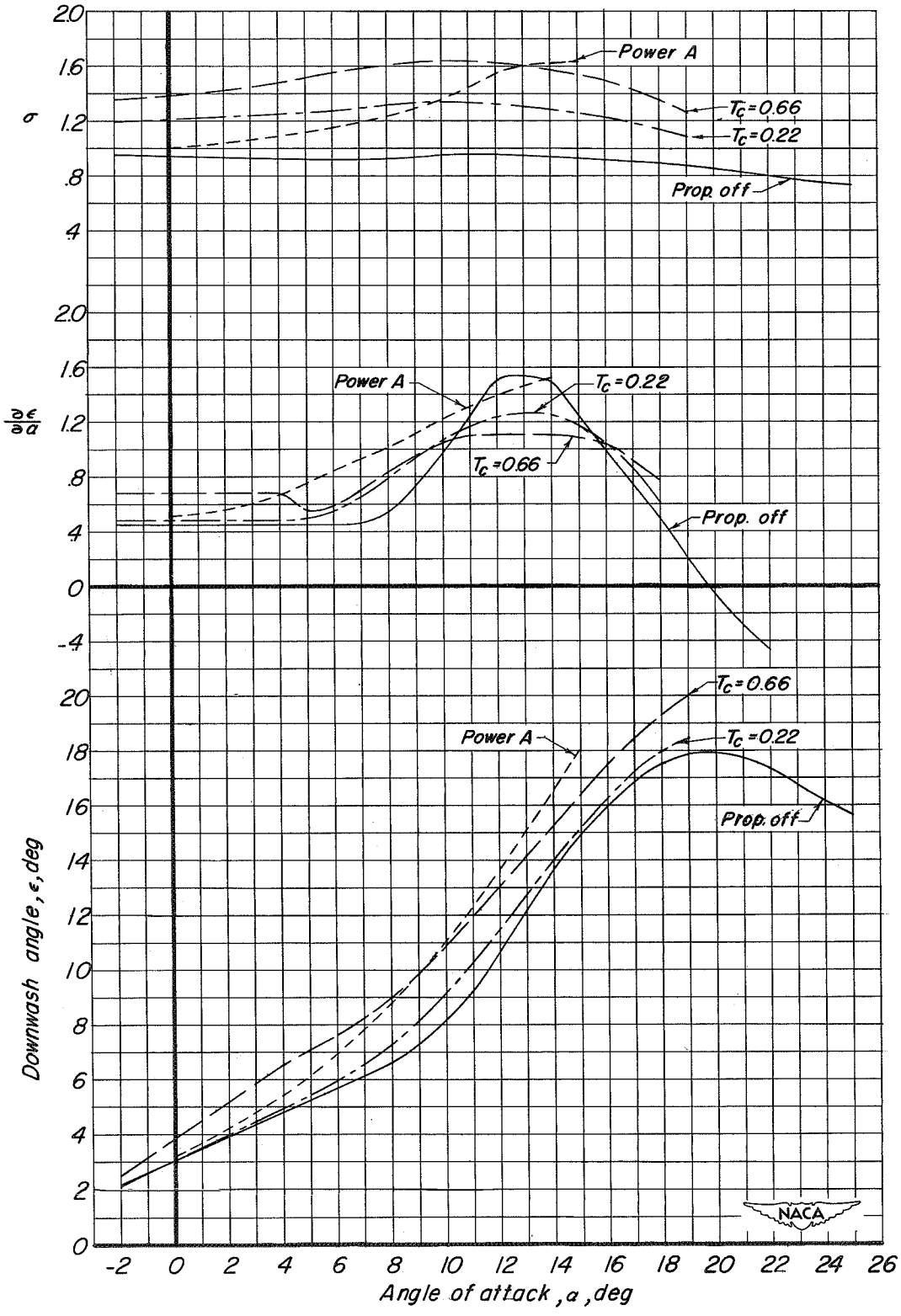

Figure 14.- Summary of effective downwash at the horizontal tail and tail effectiveness of the basic configuration. $\delta_f = 0^o$.

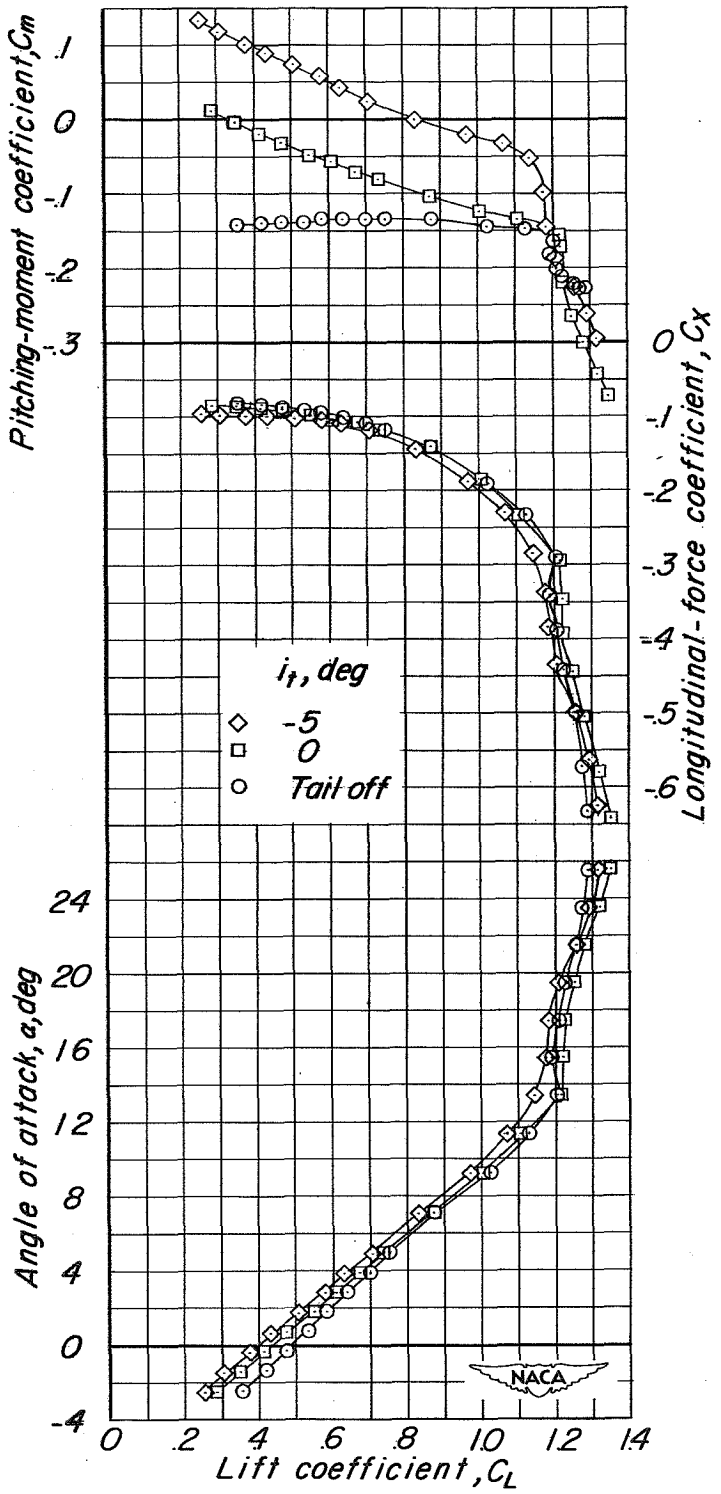

Figure 15.- Effect of stabilizer incidence on the aerodynamic characteristics of the complete model with the propeller off. Original configuration; $\delta_f = 40^\circ$; slats extended.

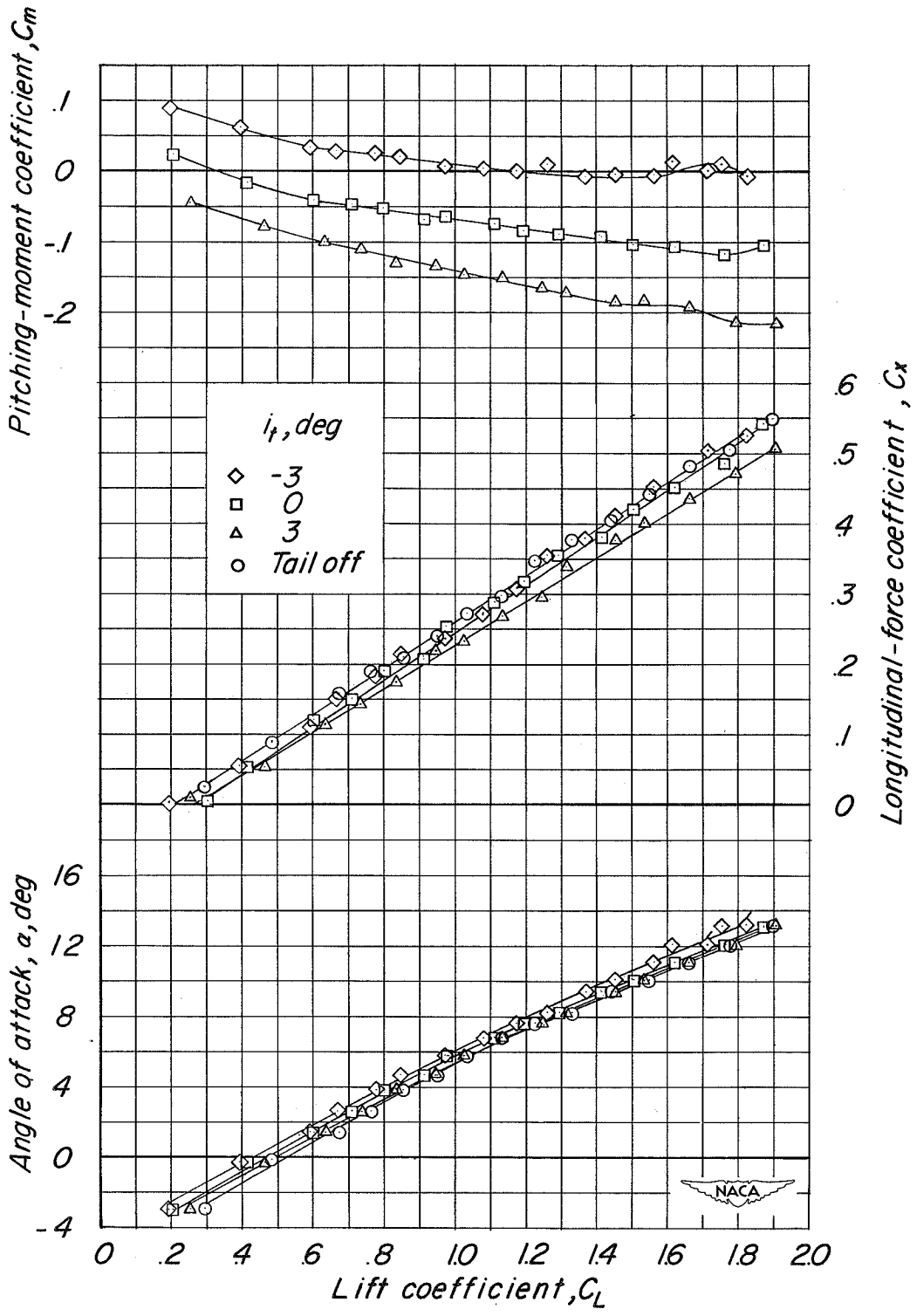

Figure 16.- Effect of stabilizer incidence on the aerodynamic characteristics of the complete model with the propeller operating. Original configuration; $\delta_f = 40^\circ$; slats extended; power B.

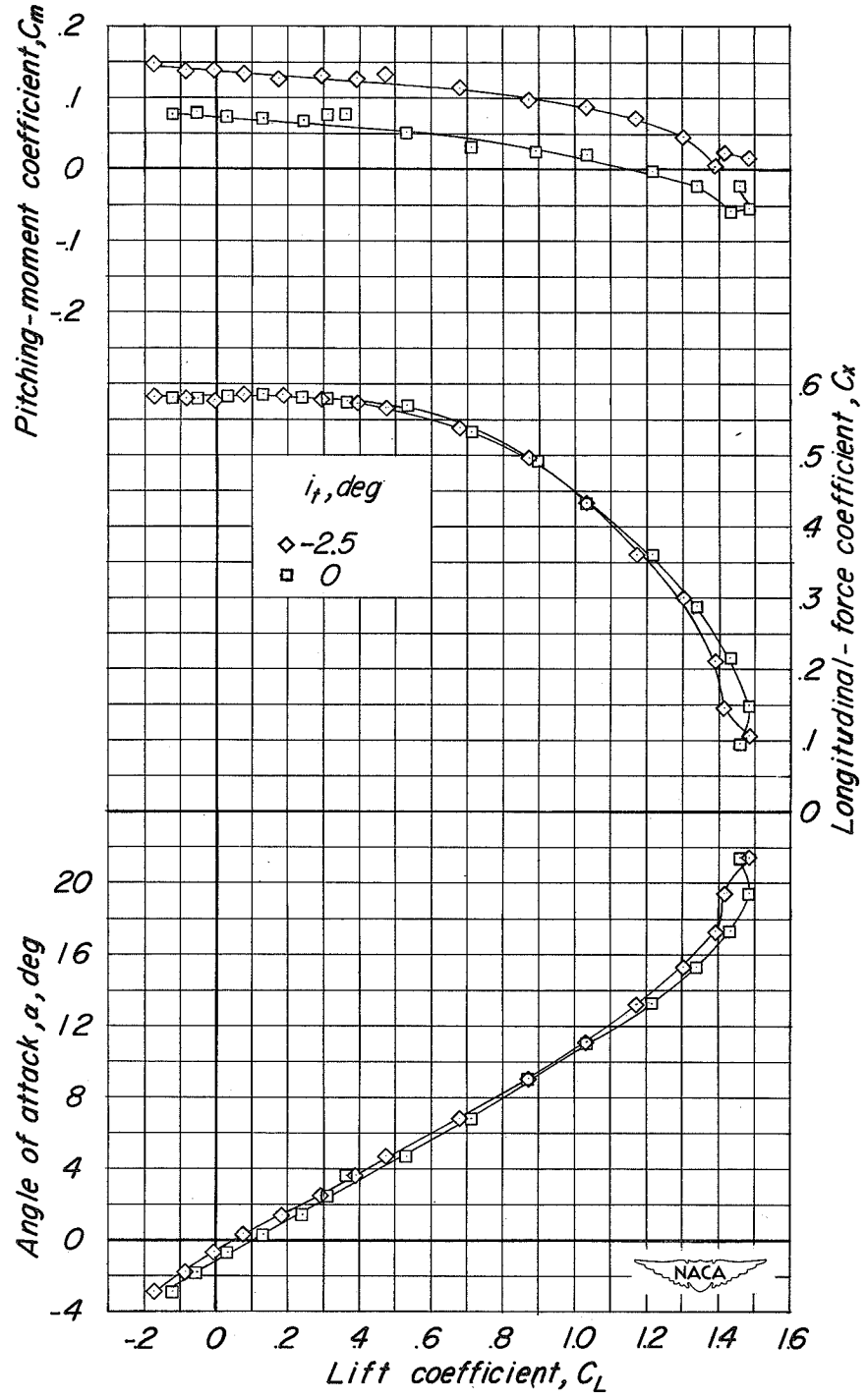

(a) $T_c = 0.66$.

Figure 17.- Effect of stabilizer incidence on the aerodynamic characteristics of the complete model with the propeller operating. Leading-edge chord-extension from 65 to 94 percent b/2; $\delta_f = 0^\circ$.

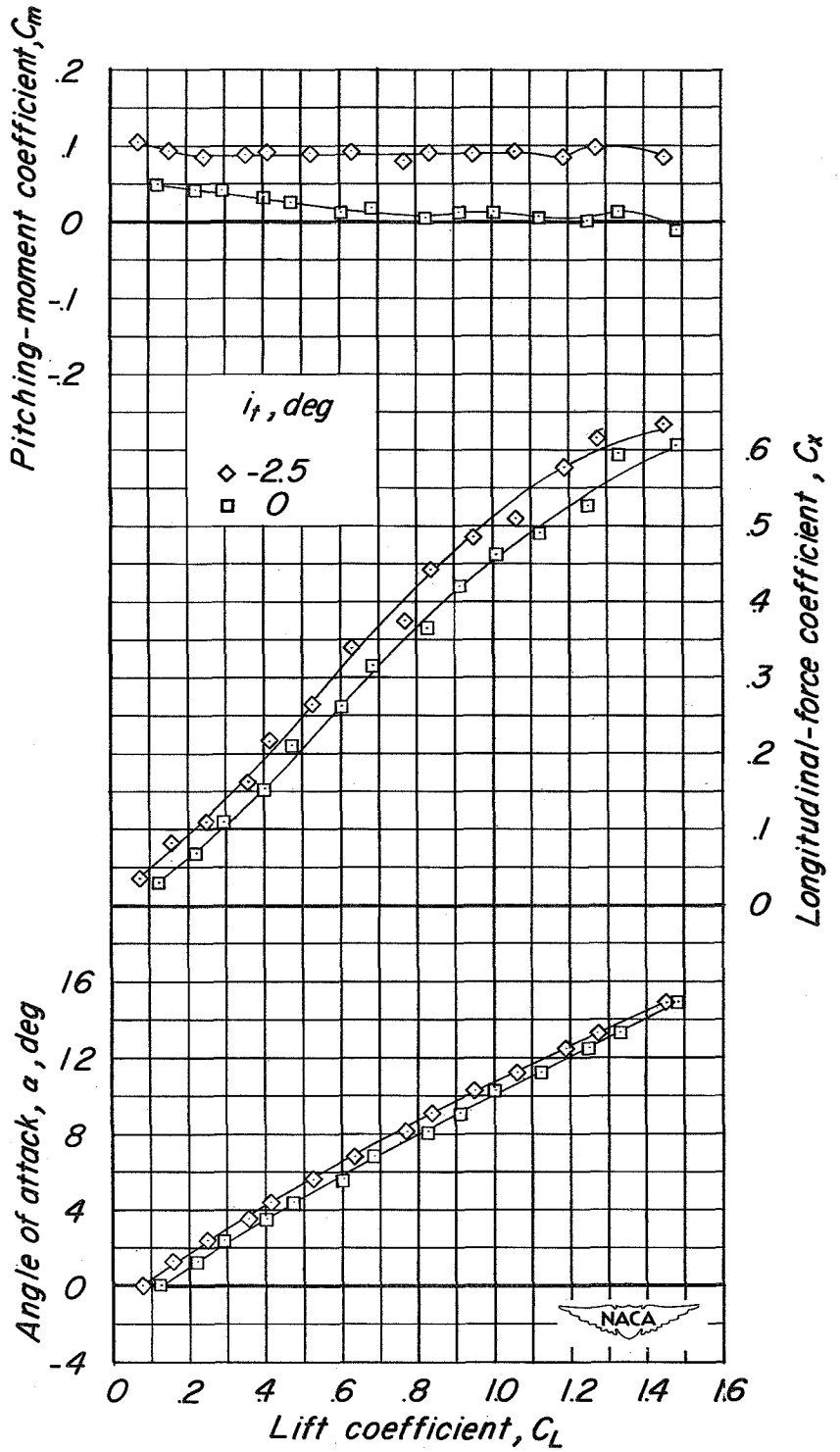

(b) Power A.

Figure 17.- Concluded.

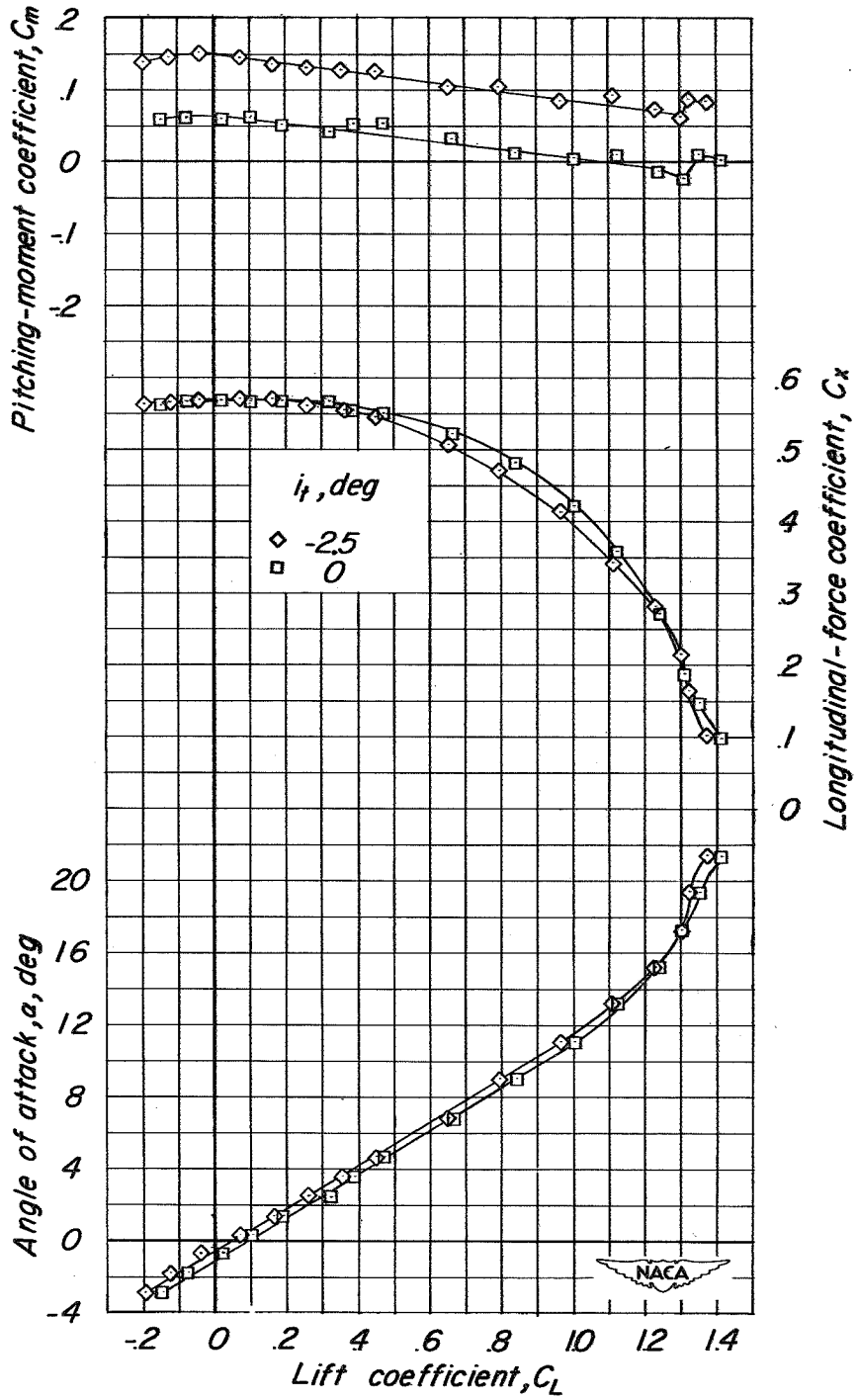

(a) $T_c = 0.66$.

Figure 18.- Effect of stabilizer incidence on the aerodynamic characteristics of the complete model with the propeller operating. Wing fence at 75 percent b/2; $\delta_f = 0^\circ$.

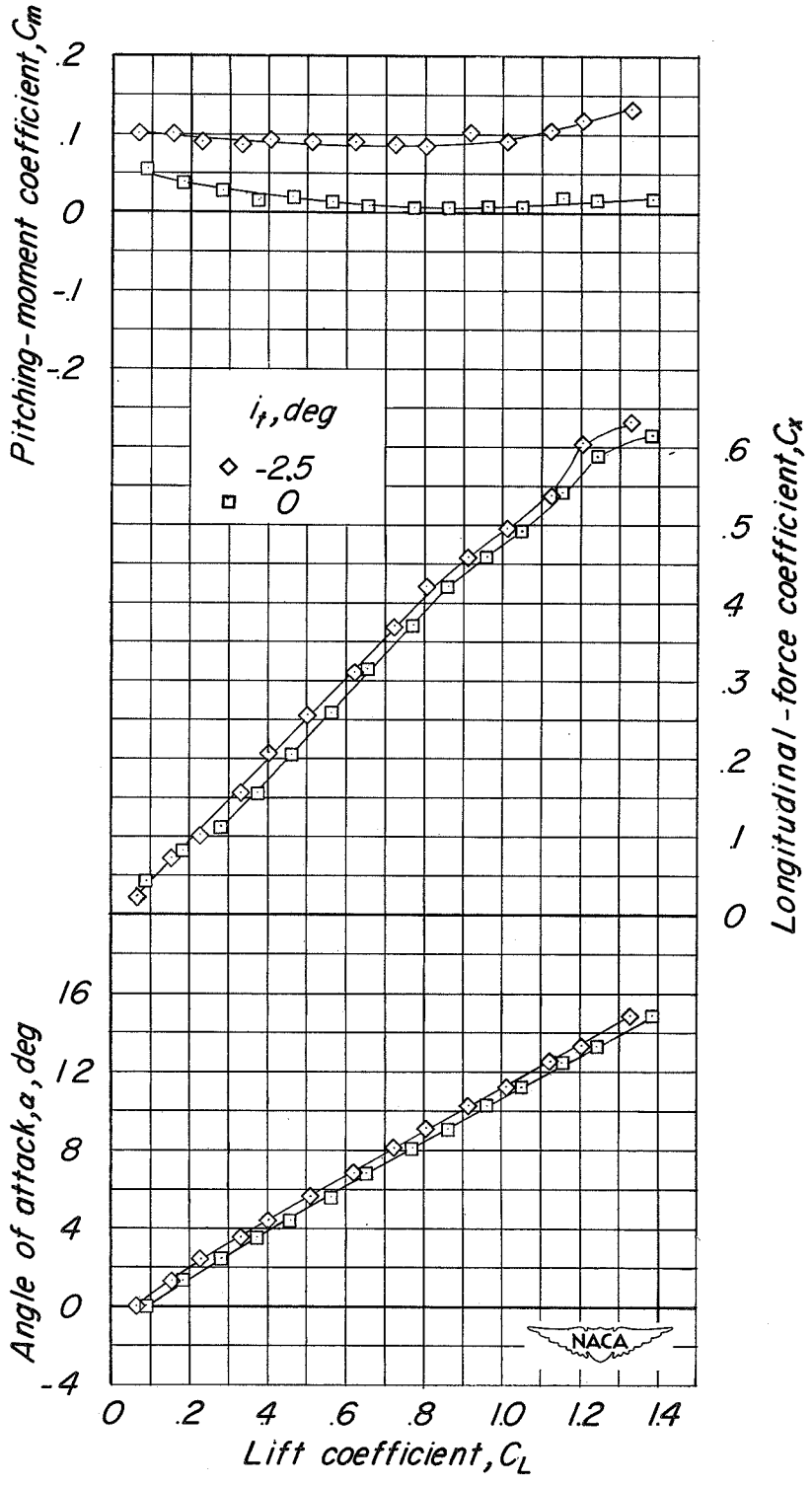

(b) Power A.

Figure 18.- Concluded.

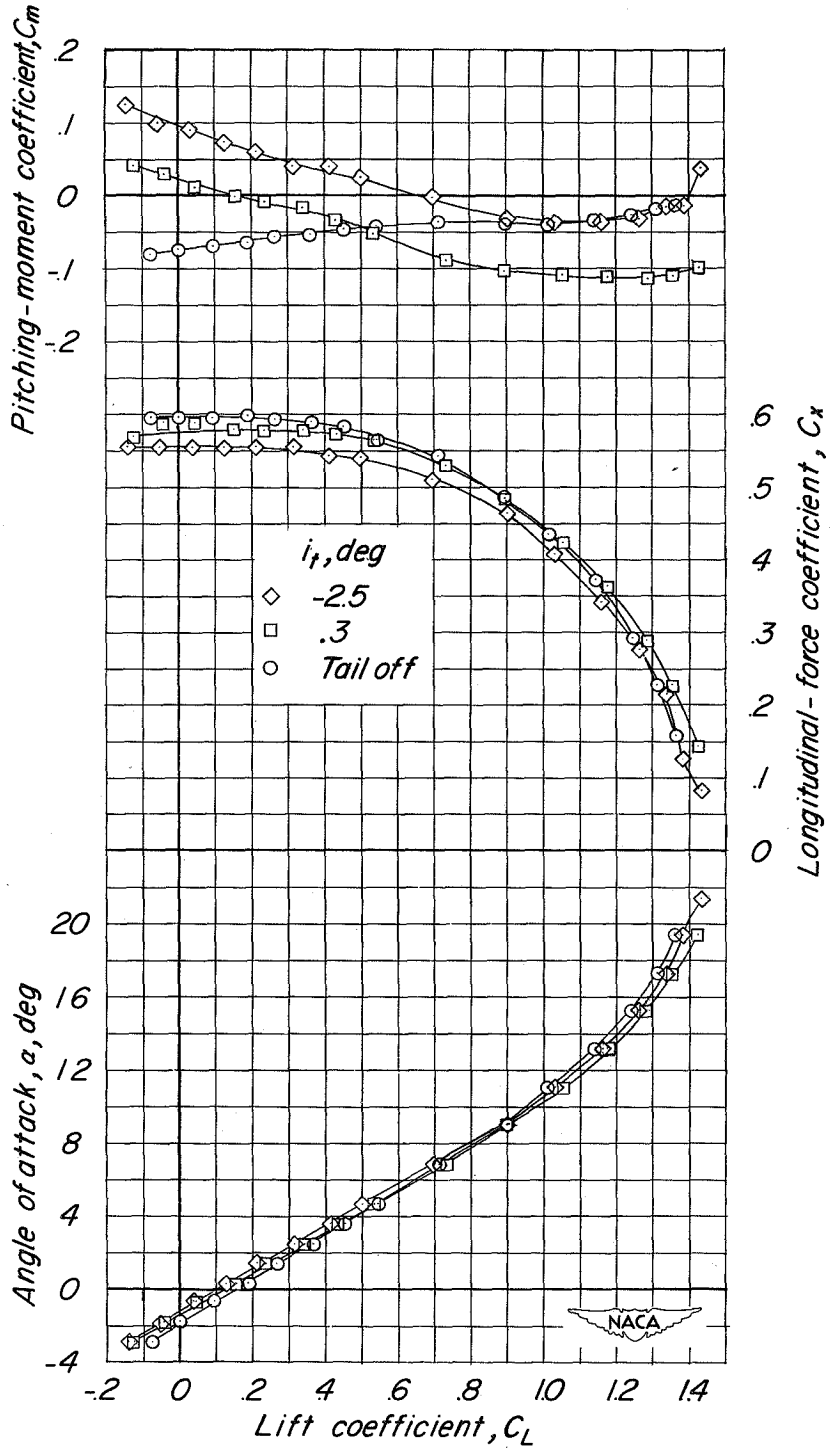

(a) $T_c = 0.66$.

Figure 19.- Effect of stabilizer incidence on the aerodynamic characteristics of the complete model with the propeller operating. High horizontal-tail position; $\delta_f = 0^\circ$.

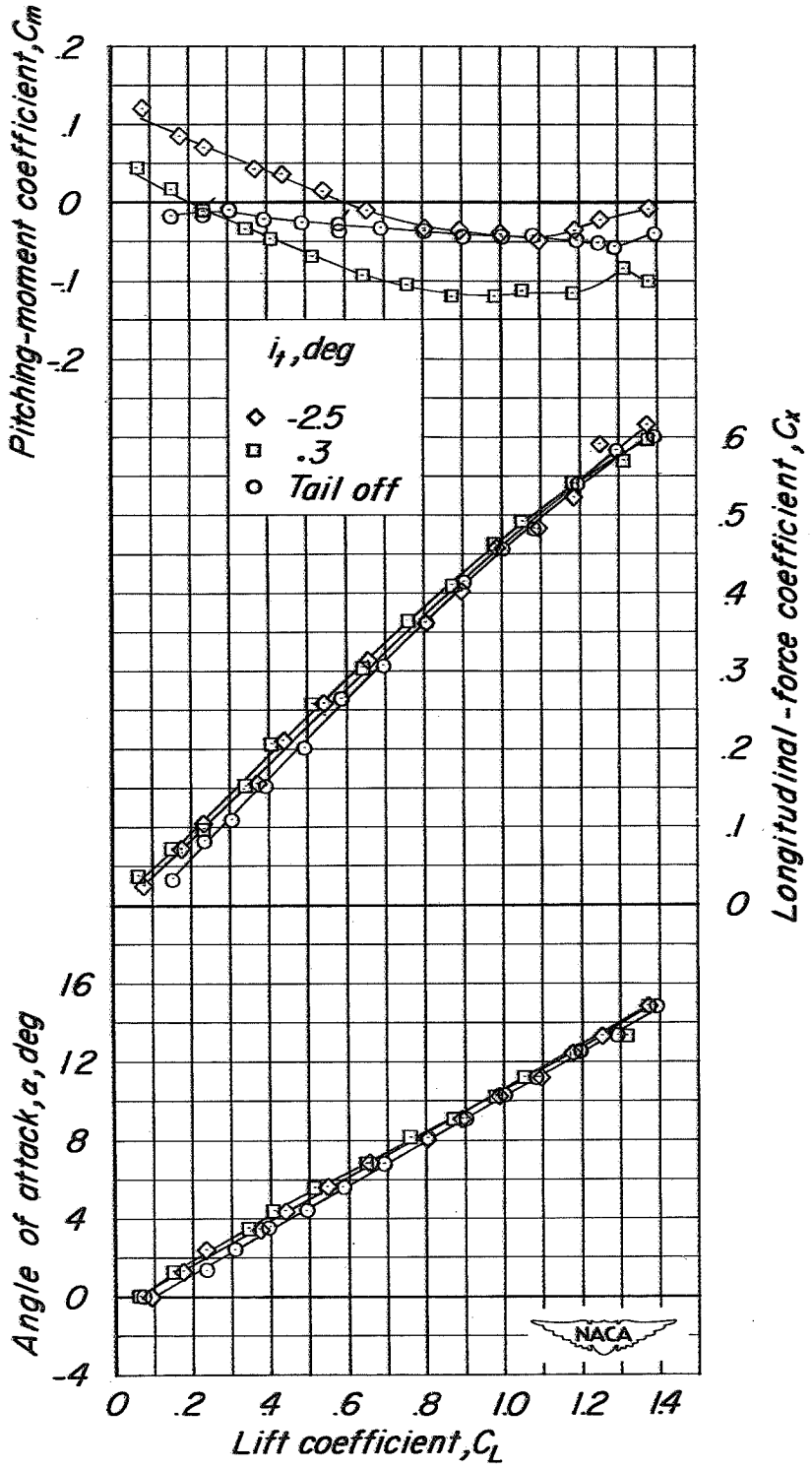

(b) Power A.

Figure 19.- Concluded.

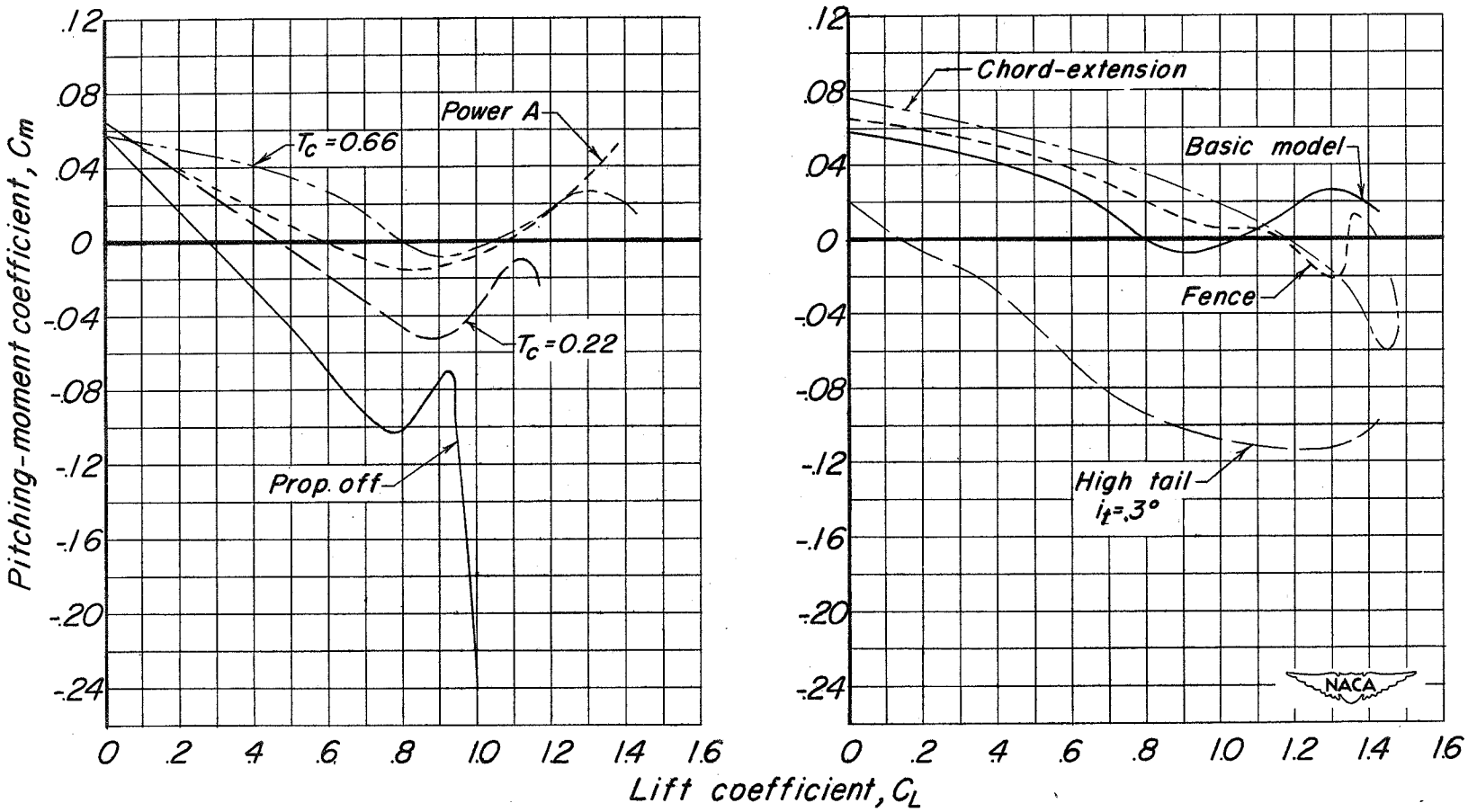

(a) Effect of power, basic configuration.

(b) Effect of wing and tail modifications. T_c = 0.66.

Figure 20.- Summary of the effects of power and modifications. $\delta_f = 0^\circ$; $i_t = 0^\circ$.

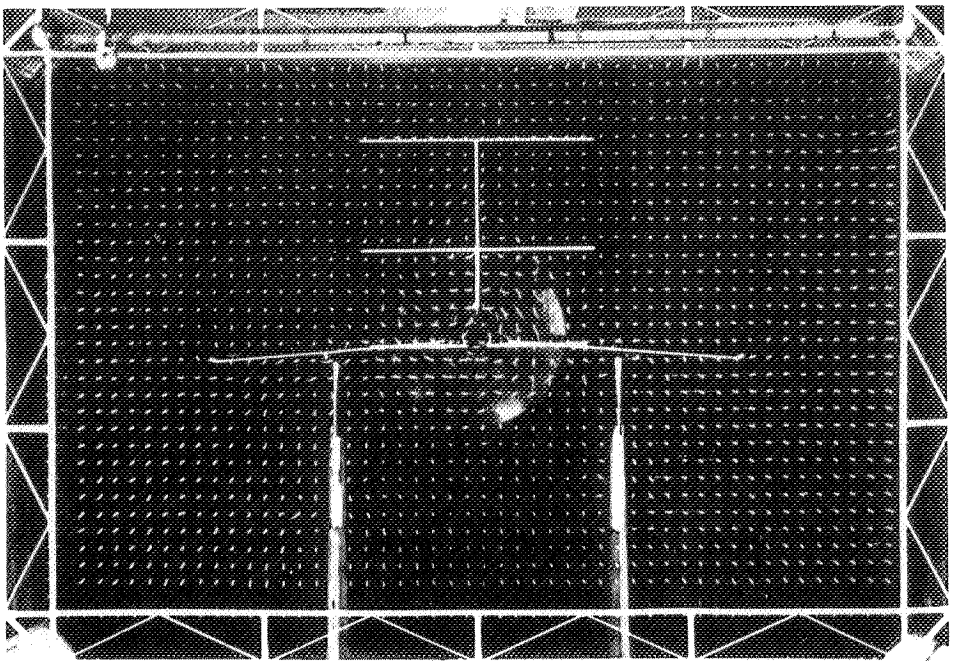

$\alpha = 0.39°$ $C_L = .134$

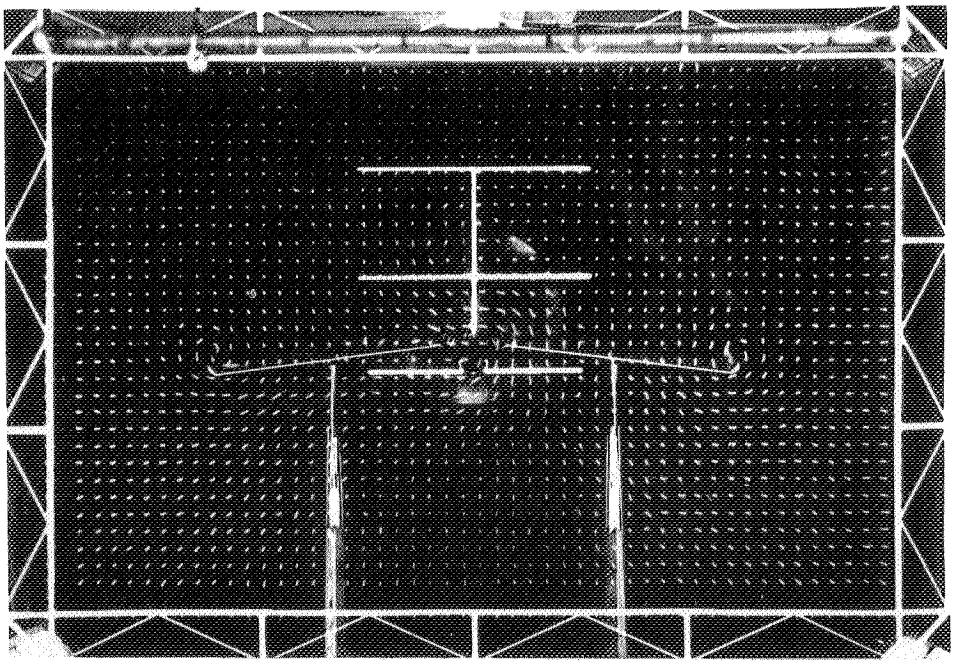

$\alpha = 4.17°$ $C_L = .540$

Figure 21.- Tuft grid photographs for the basic configuration. $\delta_f = 0°$; $T_c = 0.66$. L-80206

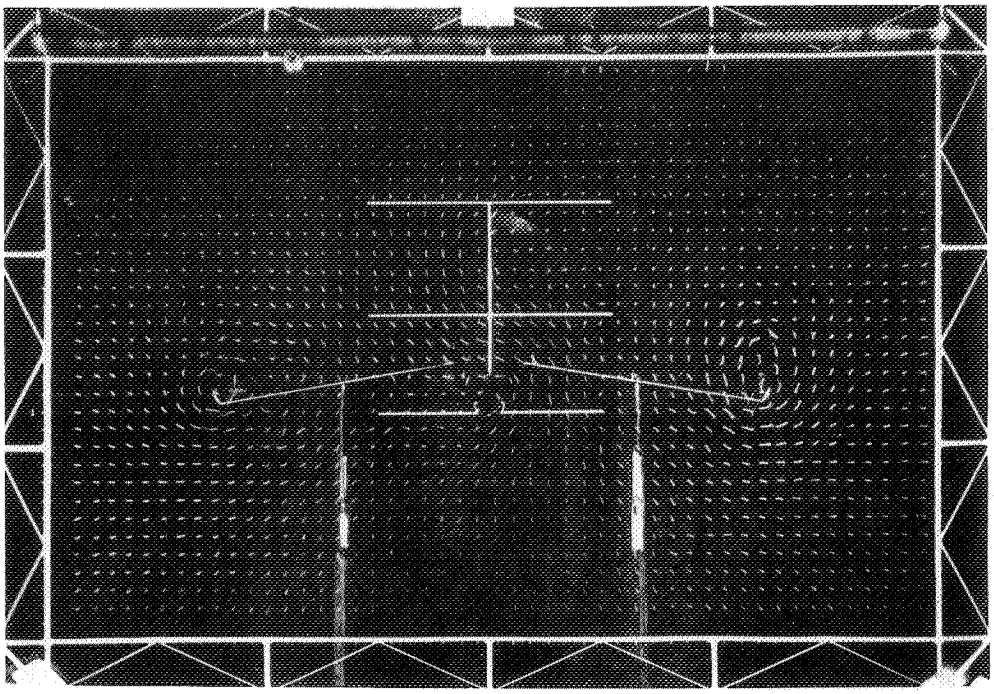

$\alpha = 9.03°$ $C_L = .887$

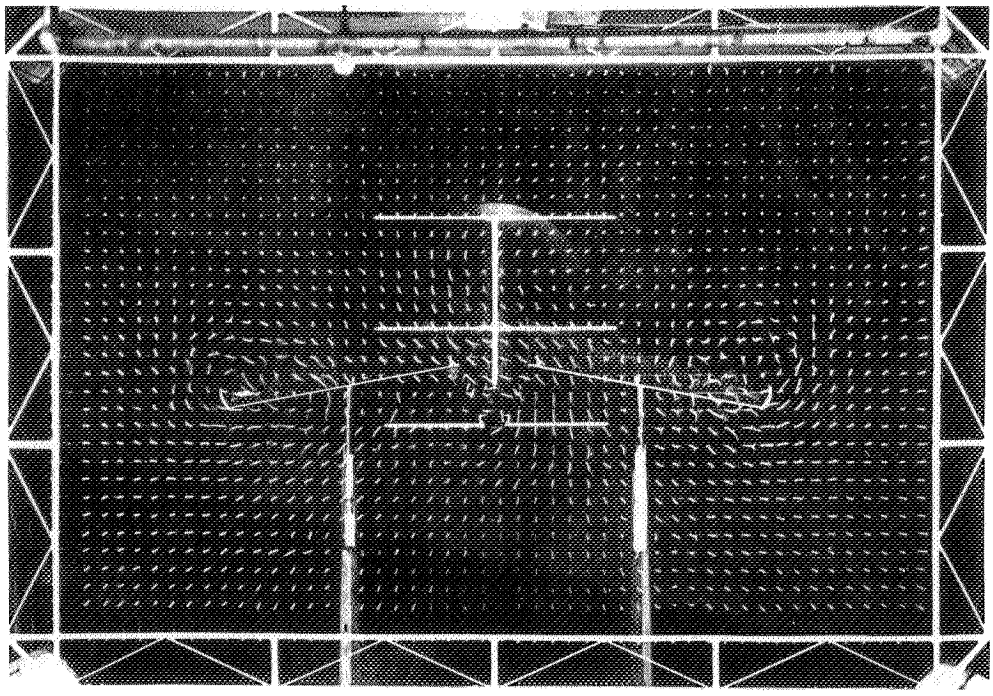

$\alpha = 11.13°$ $C_L = 1.040$

Figure 21.- Continued. L-80207

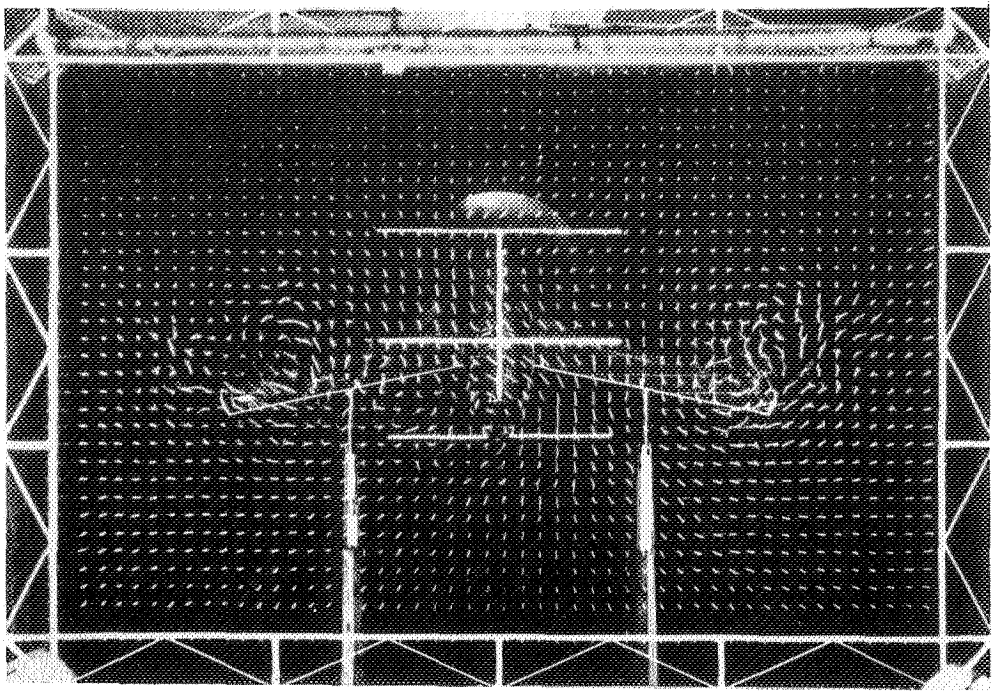

$\alpha = 13.24°$ $C_L = 1.157$

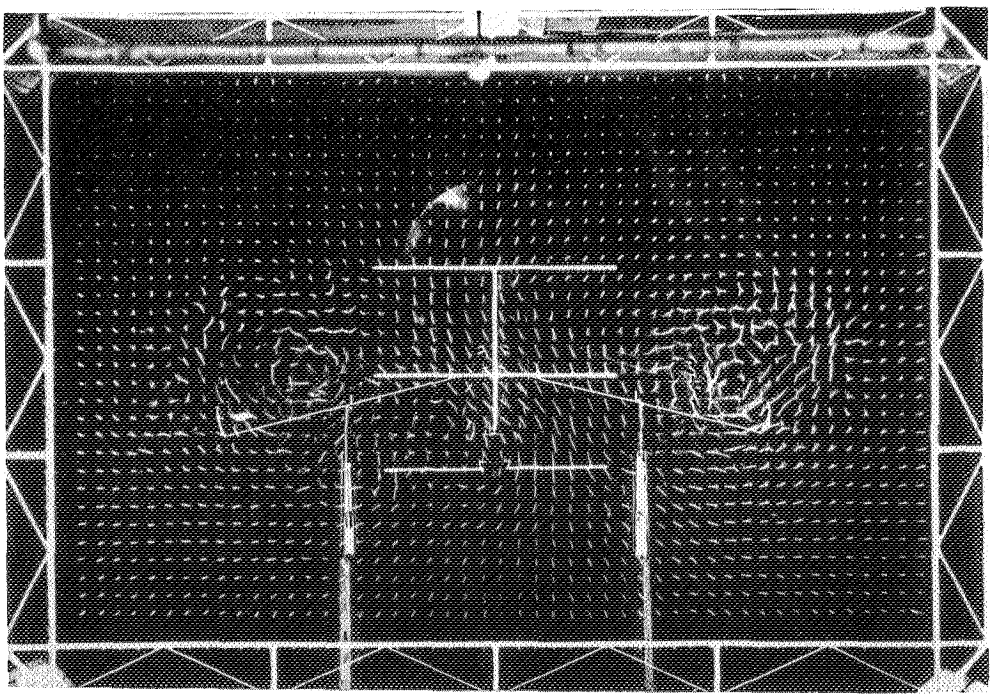

$\alpha = 17.38°$ $C_L = 1.362$

Figure 21.- Concluded. L-80208

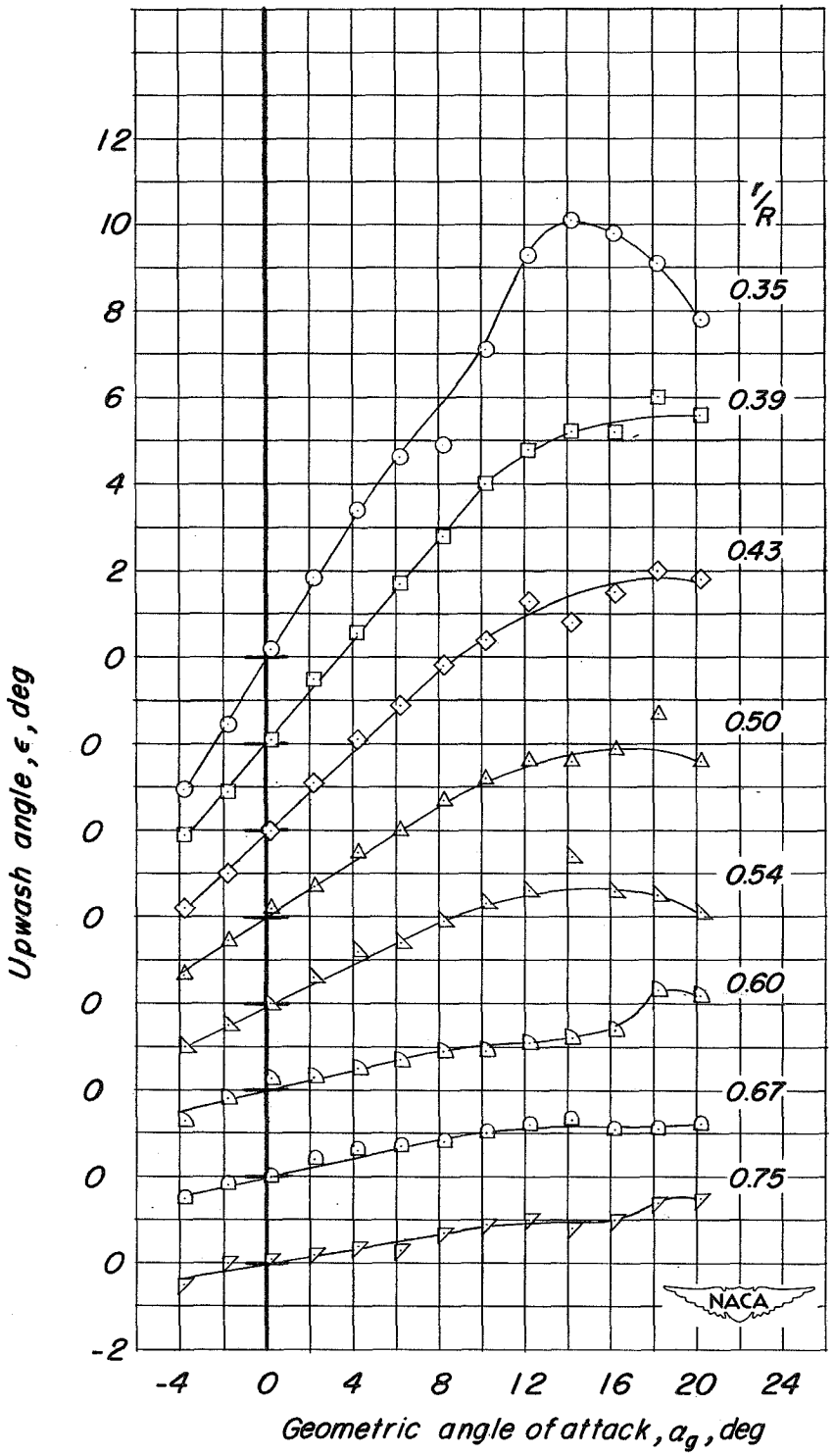

(a) Fuselage alone.

Figure 22.- Upwash angles measured in the propeller plane of the basic model, q = 40 pounds per square foot.

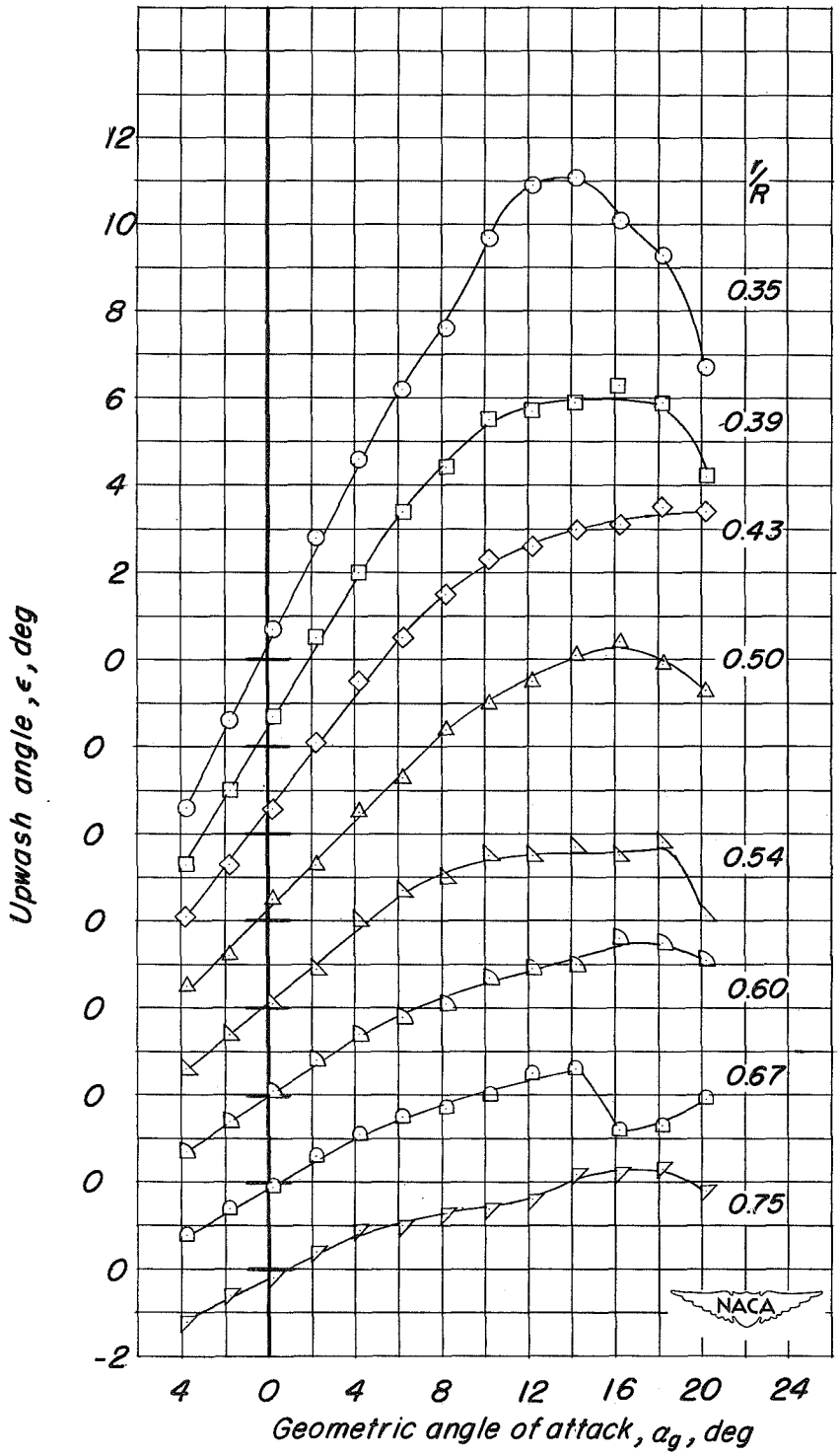

(b) Wing-fuselage, $\delta_f = 0^\circ$.

Figure 22.- Concluded.

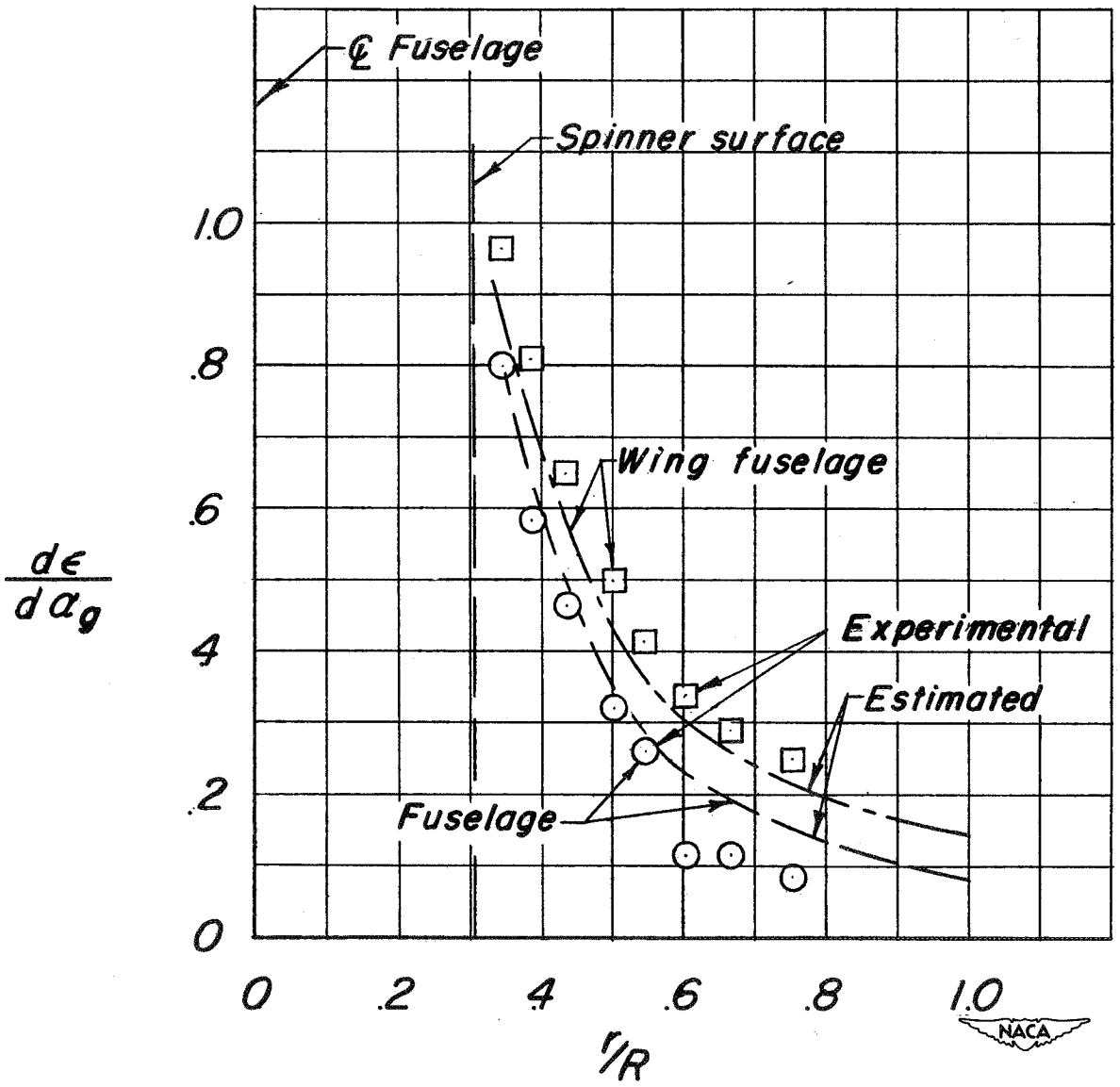

Figure 23.- Comparison of estimated and experimental upwash gradients in the propeller plane of the basic model.

NACA-Langley - 6-23-53 -50